LETTER

doi:10.1038/nature22819

Histone deacetylase 3 prepares brown adipose tissue for acute thermogenic challenge

Matthew J. Emmett[1,2*], Hee-Woong Lim[1,3*], Jennifer Jager[1,2], Hannah J. Richter[1,2], Marine Adlanmerini[1,2], Lindsey C. Peed[1,2], Erika R. Briggs[1,2], David J. Steger[1,2], Tao Ma[4,5], Carrie A. Sims[1,6], Joseph A. Baur[1,7], Liming Pei[1,8,9], Kyoung-Jae Won[1,3], Patrick Seale[1,10], Zachary Gerhart-Hines[4,5] & Mitchell A. Lazar[1,2,3]

Brown adipose tissue is a thermogenic organ that dissipates chemical energy as heat to protect animals against hypothermia and to counteract metabolic disease[1]. However, the transcriptional mechanisms that determine the thermogenic capacity of brown adipose tissue before environmental cold are unknown. Here we show that histone deacetylase 3 (HDAC3) is required to activate brown adipose tissue enhancers to ensure thermogenic aptitude. Mice with brown adipose tissue-specific genetic ablation of HDAC3 become severely hypothermic and succumb to acute cold exposure. Uncoupling protein 1 (UCP1) is nearly absent in brown adipose tissue lacking HDAC3, and there is also marked downregulation of mitochondrial oxidative phosphorylation genes resulting in diminished mitochondrial respiration. Remarkably, although HDAC3 acts canonically as a transcriptional corepressor[2], it functions as a coactivator of oestrogen-related receptor α (ERRα) in brown adipose tissue. HDAC3 coactivation of ERRα is mediated by deacetylation of PGC-1α and is required for the transcription of *Ucp1*, *Ppargc1a* (encoding PGC-1α), and oxidative phosphorylation genes. Importantly, HDAC3 promotes the basal transcription of these genes independently of adrenergic stimulation. Thus, HDAC3 uniquely primes *Ucp1* and the thermogenic transcriptional program to maintain a critical capacity for thermogenesis in brown adipose tissue that can be rapidly engaged upon exposure to dangerously cold temperature.

Brown adipose tissue (BAT) is a major site of mammalian non-shivering thermogenesis mediated through UCP1-dependent respiration[1]. Cold temperature triggers fuel oxidation and UCP1-mediated dissipation of the mitochondrial proton gradient to rapidly generate heat in BAT[1,3], and C57BL/6J (B6) mice acclimated to room temperature (22 °C) survive acute exposure to 4 °C through this mechanism[1,4]. While UCP1-deficient mice can utilize other thermogenic mechanisms upon gradual acclimation to cold[5–8], UCP1 is required to prevent lethal hypothermia upon rapid decreases in ambient temperature, such as from 22 °C to 4 °C (ref. 4). Although much is known about brown adipose commitment and differentiation[9], the transcriptional mechanisms that ensure readiness of mature BAT for immediate heat production remain unclear[10].

The ubiquitously expressed class I histone deacetylase HDAC3 is an epigenomic modulator of nuclear receptor controlled gene expression, functioning as a stoichiometric component of the nuclear receptor co-repressor (NCoR) complex[2] to modulate deacetylation of histones as well as non-histone targets[11]. Global HDAC3 deletion is embryonic lethal[12], but studies of its tissue-specific functions link HDAC3 to hepatic steatosis[13], macrophage function[14], atherosclerosis[15], bone density[16], intestinal homeostasis[17], and cardiac energy metabolism[18,19]. However, its physiological role in BAT is not known.

We bred B6 mice with a floxed HDAC3 allele to B6 mice harbouring the pan-adipose *adiponectin-cre* (*Adipoq-cre*) and the BAT-specific *Ucp1-cre* for conditional pan-adipose and BAT-specific knockout (KO) (Extended Data Fig. 1a), and challenged adults with a drop in ambient temperature from 22 °C to 4 °C. As expected, control littermates maintained their core body temperature in the face of the acute environmental change (Fig. 1a). Strikingly, both the *Adipoq-cre* and *Ucp1-cre* HDAC3 KO mice exhibited a rapid loss of core body temperature, becoming severely hypothermic within just a few hours of moving to 4 °C (Fig. 1a). The inability to maintain core body temperature was lethal for every mouse lacking HDAC3 in BAT, whereas all the control littermates survived (Fig. 1b). Notably, the severe cold susceptibility of the HDAC3 KO mice was similar to that observed in congenic *Ucp1* KO mice (Fig. 1a, b).

The requirement for HDAC3 in regulating BAT-thermogenic capacity was examined by measuring noradrenaline-induced whole-body oxygen consumption in anaesthetized mice. Control littermates exhibited a rapid and robust increase in oxygen consumption following noradrenaline treatment whereas HDAC3 KO mice had a blunted response comparable to that observed in *Ucp1* KO mice[1] (Fig. 1c). Despite severely impaired BAT metabolic respiration, loss of HDAC3 had little effect on interscapular BAT mass, BAT mitochondrial content, or total body mass (Extended Data Fig. 1b–d).

BAT mitochondrial function was tested by high-resolution respirometry. As expected, palmitoylcarnitine and pyruvate induced respiration in control BAT mitochondria and, consistent with UCP1-dependence, this was inhibited by guanosine diphosphate[1] (Fig. 1d). Remarkably, mitochondria from HDAC3 KO BAT exhibited impaired substrate-induced respiration, with reduced function of complexes I, II, and IV of the electron transport chain (Fig. 1d). Consistent with this mitochondrial dysfunction, histological analysis revealed the presence of larger lipid droplets in HDAC3 KO BAT (Fig. 1e). By contrast, the histology of inguinal white adipose tissue (iWAT) lacking HDAC3 was similar to that of wild-type (WT) mice (Extended Data Fig. 1e),

To elucidate the molecular basis through which HDAC3 controls the thermogenic capacity of BAT, we next performed RNA sequencing (RNA-seq) on BAT from control and KO mice housed at thermoneutrality (29 °C) to avoid the potentially confounding influence of cold-stress. Consistent with the well-known function of HDAC3 as a corepressor, many genes were induced by loss of HDAC3, including

[1]Institute for Diabetes, Obesity, and Metabolism, Perelman School of Medicine at the University of Pennsylvania, Philadelphia, Pennsylvania 19104, USA. [2]Division of Endocrinology, Diabetes, and Metabolism, Department of Medicine, Perelman School of Medicine at the University of Pennsylvania, Philadelphia, Pennsylvania 19104, USA. [3]Department of Genetics, Perelman School of Medicine at the University of Pennsylvania, Philadelphia, Pennsylvania 19104, USA. [4]Section for Metabolic Receptology, Novo Nordisk Foundation Center for Basic Metabolic Research, University of Copenhagen, Copenhagen 2200, Denmark. [5]Institute for Neuroscience and Pharmacology, University of Copenhagen, Copenhagen 2200, Denmark. [6]The Trauma Center at Penn, Department of Surgery, Perelman School of Medicine at the University of Pennsylvania, Philadelphia, Pennsylvania 19104, USA. [7]Department of Physiology, Perelman School of Medicine at the University of Pennsylvania, Philadelphia, Pennsylvania 19104, USA. [8]Center for Mitochondrial and Epigenomic Medicine, Children's Hospital of Philadelphia, Philadelphia, Pennsylvania 19104, USA. [9]Department of Pathology and Laboratory Medicine, Perelman School of Medicine at the University of Pennsylvania, Philadelphia, Pennsylvania 19104, USA. [10]Department of Cell and Developmental Biology, Perelman School of Medicine at the University of Pennsylvania, Philadelphia, Pennsylvania 19104, USA.
*These authors contributed equally to this work.

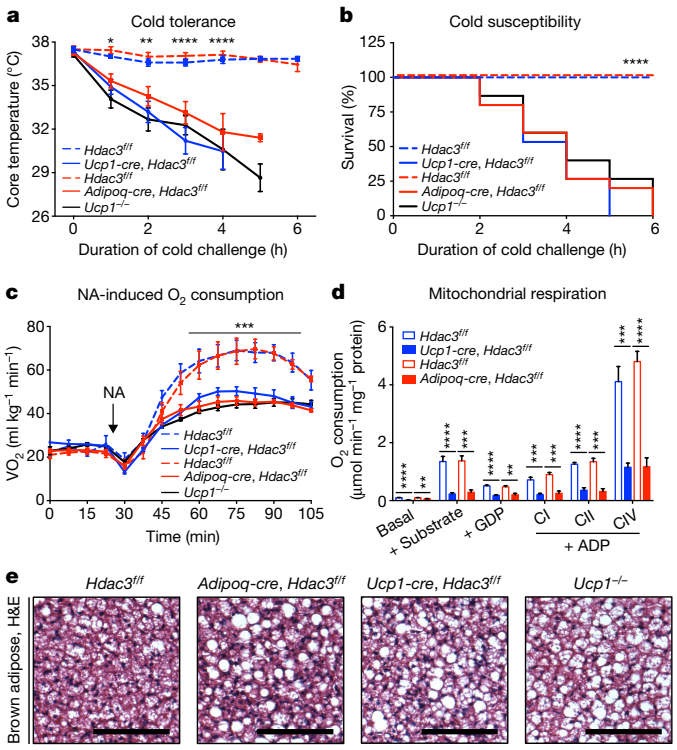

Figure 1 | HDAC3 controls BAT thermogenesis. a, **b**, Effect of acute cold exposure from standard housing at 22 °C to 4 °C on *Adipoq-cre* HDAC3 KO (*Hdac3*$^{f/f}$) mice versus control littermates ($n = 15, 8$), *Ucp1-cre* HDAC3 KO mice versus control littermates ($n = 15, 7$), and *Ucp1*$^{-/-}$ mice ($n = 15$): **a**, core body temperature; **b**, survival. **c**, Oxygen consumption rates of anaesthetized *Adipoq-cre* HDAC3 KO mice versus control littermates ($n = 12, 5$), *Ucp1-cre* HDAC3 KO mice versus control littermates ($n = 6, 5$), and *Ucp1*$^{-/-}$ mice ($n = 5$) after injection of 1 mg per kg (body weight) noradrenaline (NA). **d**, Mitochondrial respiration of purified BAT homogenates from *Adipoq-cre* HDAC3 KO mice versus control littermates ($n = 5, 6$), and *Ucp1-cre* HDAC3 KO mice versus control littermates ($n = 6, 5$), after brief acclimation to thermoneutrality. Mitochondria were provided palmitoylcarnitine and pyruvate substrates. UCP1-dependent respiration was assessed upon addition of guanosine diphosphate (GDP), and coupled respiration rates of complexes I, II, and IV (CI, CII, CIV) were determined in the presence of adenosine diphosphate (ADP). **e**, Representative haematoxylin and eosin (H&E) staining of interscapular brown adipose from 10- to 12-week-old mice at 22 °C. Scale bars, 100 μm. $^{*}P < 0.05$, $^{**}P < 0.01$, $^{***}P < 0.001$, $^{****}P < 0.0001$ as analysed by two-way analysis of variance (ANOVA) with a Tukey's post hoc test (**a**, **c**), log-rank (Mantel–Cox) test (**b**), or two-tailed Student's *t*-test (**d**). Data are represented as mean ± s.e.m.

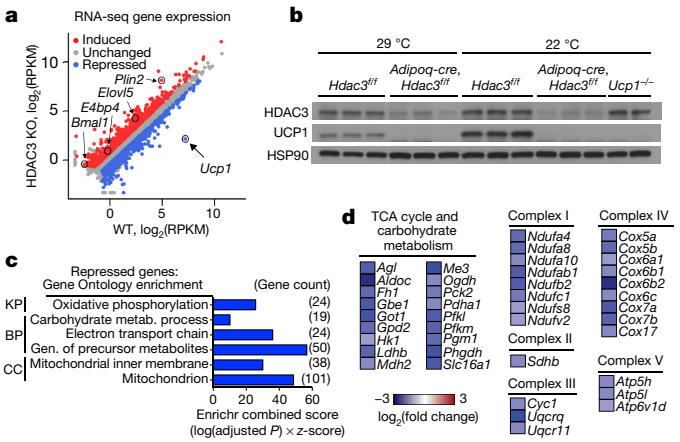

Figure 2 | HDAC3 is required for expression of UCP1 and OXPHOS genes in BAT. a, Scatter plot of RNA-seq data showing HDAC3-regulated BAT genes from *Adipoq-cre* HDAC3 KO versus control littermates ($n = 4, 4$) adapted to thermoneutrality (fold change >1.5 up (red) or down (blue) and false discovery rate (FDR) < 0.01). RPKM, reads per kilobase per million. **b**, Immunoblot from BAT of *Adipoq-cre* HDAC3 KO mice, control littermates, or *Ucp1*$^{-/-}$ mice adapted to 29 °C or maintained at 22 °C ($n = 3, 3$; $n = 3, 3$; $n = 2$). **c**, Gene Ontology and pathway analysis of downregulated genes identified by RNA-seq and selected by Enrichr combined score (KP, KEGG Pathway; BP, Biological Process; CC, Cellular Component); metab., metabolism; Gen., generation. **d**, Heat map depicting downregulated genes identified in Gene Ontology analysis.

classic repression targets of the nuclear receptor Rev-erbα such as *Bmal1* (also known as *Arntl*), *E4bp4* (also known as *Nfil3*), *Elovl5*, and *Plin2* (Fig. 2a). However, many genes were also decreased in HDAC3 KO BAT, including a near-complete loss of *Ucp1* in the BAT of HDAC3 KO animals (Fig. 2a). UCP1 protein expression was nearly undetectable in HDAC3 KO BAT, at both 29 °C and 22 °C (Fig. 2b). *Ucp1* expression remained low in HDAC3 KO BAT after acute cold exposure (Extended Data Fig. 2a, b) although it was induced in iWAT (Extended Data Fig. 2c, d), suggesting a BAT-selective requirement for HDAC3. BAT HDAC3 messenger RNA (mRNA) and protein levels were not appreciably affected by acute cold exposure (Extended Data Fig. 2e, f), and HDAC3 was neither induced nor required for primary brown adipocyte differentiation (Extended Data Fig. 3a–d). However, primary brown adipocytes lacking HDAC3 exhibited reduced basal *Ucp1*, which was minimally responsive to isoproterenol (Extended Data Fig. 3e–g), demonstrating a cell-autonomous effect of HDAC3.

Analysis of the genes repressed by HDAC3 KO in BAT revealed a strong enrichment for thermogenic pathways, including mitochondrial oxidative phosphorylation, tricarboxylic acid cycle (TCA) enzymes, and other metabolic and energy producing processes, with no signal for inflammatory pathways (Fig. 2c). Many components of the TCA cycle and complexes I–V of the electron transport chain were diminished in the absence of HDAC3 (Fig. 2d and Extended Data Fig. 4a), as confirmed by reverse-transcription–quantitative PCR (RT–qPCR) at both 29 °C and 22 °C in pan-adipose as well as BAT-specific HDAC3 KO models (Extended Data Fig. 4b, c).

Relative to controls, BAT HDAC3 KO animals had similar body weight and lean mass, with slightly less body fat but indistinguishable basal energy expenditure, activity, and food intake at 22 °C (Extended Data Fig. 5). Moreover, after 12 weeks of high-fat feeding at room temperature, pan-adipose and BAT-specific HDAC3 KO mice gained similar amounts of weight and body fat relative to controls (Extended Data Fig. 6a–d), whose BAT HDAC3 expression was indistinguishable from mice fed with regular chow (Extended Data Fig. 6e). These findings are similar to the phenotype of *Ucp1* KO mice[4], and suggestive of *Ucp1*-independent mechanisms that may control energy expenditure and body weight[5–8]. Thus, HDAC3 is uniquely required for priming the mitochondrial oxidative and thermogenic energy-expending gene programs in classic BAT to defend against environmental cold.

To determine the mechanism by which HDAC3 drives expression of thermogenic gene pathways, we performed chromatin immunoprecipitation followed by sequencing (ChIP–seq) in BAT for HDAC3 and for acetylated histone H3 lysine 27 (H3K27ac) as a marker of active enhancers[20]. Loss of HDAC3 led to reduced H3K27ac at many sites of HDAC3 binding in control mice, often near genes that were repressed by HDAC3 depletion (Fig. 3a). These results imply that, at these sites, the usual function of HDAC3 as a histone deacetylase was overridden by its function as a coactivator. By contrast, H3K27ac was increased at HDAC3 bound sites near genes that were induced in HDAC3 KO BAT (Fig. 3a).

Steady-state mRNA levels correlated well with nascent transcription at gene bodies as assessed by global run-on sequencing (GRO-seq)[21] (Extended Data Fig. 7a). Mining of the GRO-seq data for non-coding enhancer RNA (eRNA) transcription to map functional enhancers[22,23]

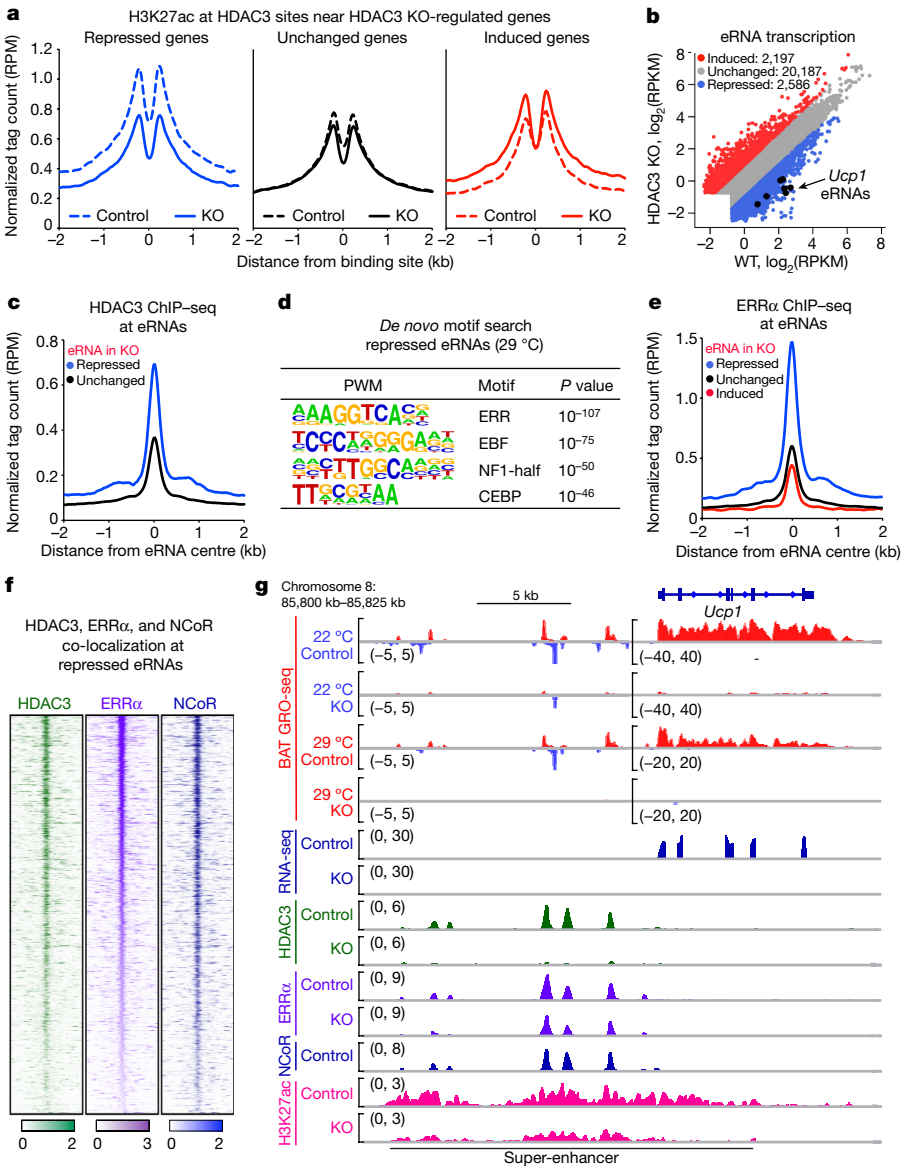

Figure 3 | HDAC3 functions as an ERRα coactivator in BAT. a, Average H3K27ac ChIP–seq profiles of *Adipoq-cre* HDAC3 KO mice versus control littermates ($n = 3, 3$; pooled biological replicates per library) at enhancers bound by HDAC3 within 100 kilobases (kb) of transcription start sites of HDAC3 KO-regulated genes by GRO-seq (fold change >1.5 or <0.5). Decreased H3K27ac at HDAC3 sites near repressed genes ($n = 1{,}085$, $P = 1.0 \times 10^{-123}$) and increased H3K27ac at HDAC3 sites near induced genes ($n = 897$, $P = 9.0 \times 10^{-56}$) upon loss of HDAC3. RPM, reads per million. **b**, Scatter plot of enhancer RNAs (eRNAs) measured by GRO-seq in *Adipoq-cre* HDAC3 KO mice versus control littermates ($n = 10, 10$; pooled biological replicates per library) at 29 °C, highlighting induced and repressed eRNAs (red, fold change >2; blue, fold change <0.5). **c**, Average HDAC3 ChIP–seq profile of control littermates ($n = 5$, pooled biological replicates per library) at enhancers with repressed or unchanged eRNAs in HDAC3 KO. Significant HDAC3 binding found at HDAC3 KO-repressed eRNAs relative to unchanged eRNAs ($P = 2.4 \times 10^{-215}$). **d**, *De novo* motif search at eRNA sites repressed in HDAC3 KO at 29 °C (ranked by *P* value). PWM, position weight matrix. **e**, Average ERRα ChIP–seq profile in control littermates ($n = 5$, pooled biological replicates per library) at enhancers with differential eRNAs in HDAC3 KO. Significant ERRα found at HDAC3 KO-repressed eRNAs relative to unchanged eRNAs ($P = 1.0 \times 10^{-288}$). **f**, Heat map depicting HDAC3, ERRα, and NCoR co-localization at enhancers with repressed eRNAs in HDAC3 KO mice (in RPM scale). **g**, Genome browser tracks of the *Ucp1* super-enhancer locus highlighting GRO-seq (22 °C, 29 °C), RNA-seq (29 °C), and ChIP–seq (29 °C) data (*y* axis scales in brackets: reads per million; eRNA tracks feature adjusted *y* axis scale). *P* values for ChIP–seq or motif search determined by Wilcoxon or binomial test, respectively.

revealed pronounced reduction in activity of multiple enhancers at the *Ucp1* locus (Fig. 3b). Genome-wide, HDAC3 binding at eRNAs that were downregulated upon HDAC3 KO was enriched in BAT of control mice, adding to the evidence that HDAC3 functioned as a coactivator at these enhancers (Fig. 3c). Since *Rev-erbα* (also known as *Nr1d1*) deletion has the opposite effect on *Ucp1* (ref. 24), we reason that the ability of HDAC3 to function as Rev-erbα corepressor must be overcome by HDAC3 coactivation of a different transcription factor.

To identify the transcription factor(s) coactivated by HDAC3, we used genome-wide *de novo* motif analysis at sites of eRNA downregulation in HDAC3 KO BAT, revealing enrichment of the binding motif for ERR at both 29 °C and 22 °C (Fig. 3d and Extended Data Fig. 7b). ERRs are potent activators of mitochondrial metabolism, oxidative phosphorylation (OXPHOS) pathways, and energy metabolism[25]. Other enriched motifs included those of known adipose lineage factors[26] including the BAT-specific EBF2 (ref. 27). Confirming the motif prediction, genome-wide ERRα binding in BAT was strongest at sites where eRNAs were downregulated upon HDAC3 KO (Fig. 3e). On a genome-wide level, HDAC3 and ERRα binding strongly co-localized along with NCoR at downregulated enhancers (Fig. 3f), suggesting a

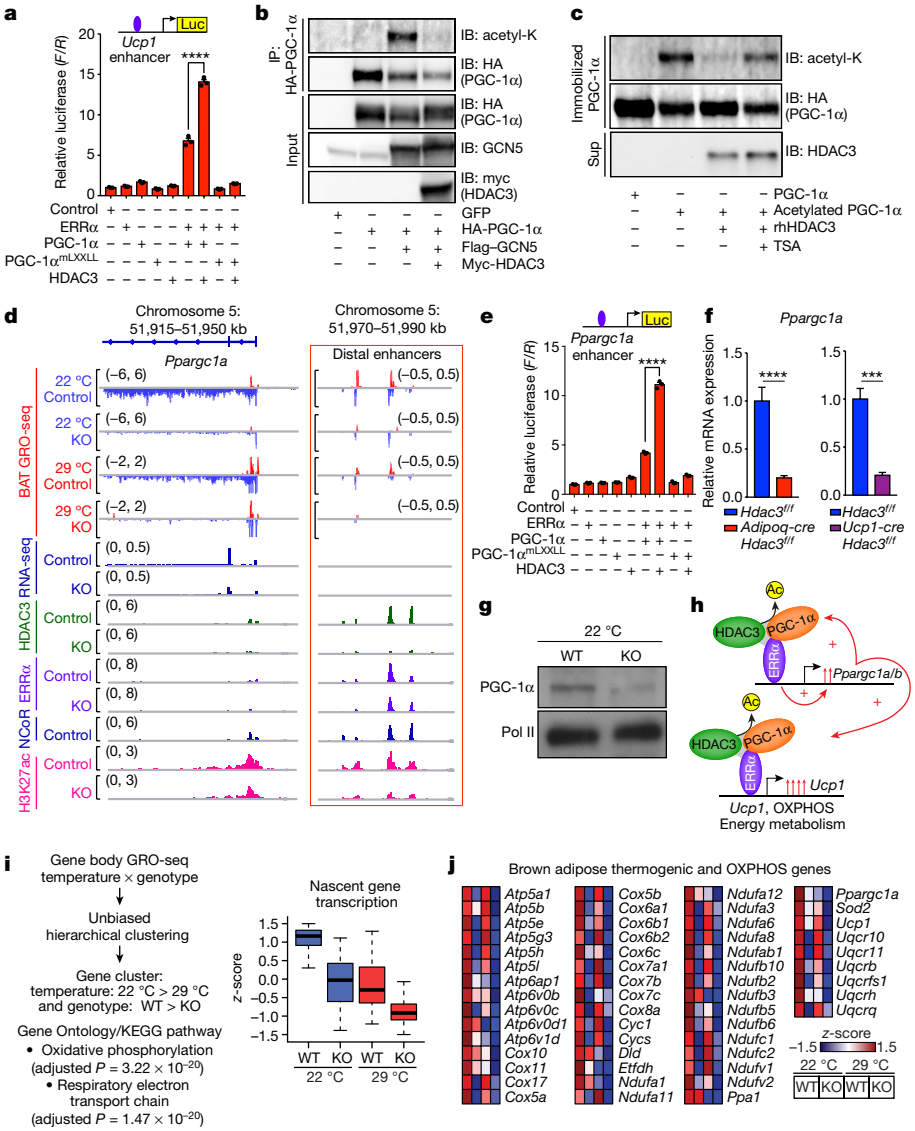

Figure 4 | HDAC3 coactivation of ERRα is mediated by PGC-1α deacetylation. a, Luciferase reporter assay of transcription driven by an identified *Ucp1* enhancer (−6 kb), demonstrating effects of ERRα, HDAC3, WT PGC-1α, and/or a PGC-1α LXXLL mutant (L1/2/3A) unable to interact with ERRα ($n = 3$ replicates per condition). **b**, Immunoblot (IB) analysis of PGC-1α lysine acetylation after immunoprecipitation from co-transfected HEK-293FT cells. HA, haemagglutinin. **c**, Immunoblot analysis of an *in vitro* deacetylation reaction of purified acetylated PGC-1α by recombinant human HDAC3, with or without trichostatin A (TSA). **d**, Genome browser tracks of the *Ppargc1a* locus highlighting GRO-seq and RNA-seq data, and eRNAs at HDAC3, ERRα, and NCoR co-bound distal enhancers (boxed). **e**, Luciferase reporter assay as in **a** for identified *Ppargc1a* distal enhancer (−38 kb), ($n = 3$ replicates per condition). **f**, BAT *Ppargc1a* mRNA from *Adipoq-cre* HDAC3 KO mice versus control littermates ($n = 9, 6$) and *Ucp1-cre* HDAC3 KO mice versus control littermates ($n = 5, 6$). **g**, Immunoblot of PGC-1α in BAT nuclear extract of *Adipoq-cre* HDAC3 KO versus control littermates ($n = 5$, pooled biological replicates per lane). **h**, BAT HDAC3 deacetylates PGC-1α to coactivate an ERR-driven transcriptional loop of *Ppargc1a/Ppargc1b*, *Ucp1*, and OXPHOS genes. **i**, Flow chart depicting unbiased hierarchical gene clustering of GRO-seq gene transcription by temperature and genotype. Box plot displays gene cluster requiring HDAC3 coactivator function, where line denotes median, top/bottom of boxes represents first/third quartiles, and whiskers denote 1.5 times the interquartile range from first/third quartiles. **j**, Heat map of thermogenic and OXPHOS genes identified in **i**. $^{***}P < 0.001$, $^{****}P < 0.0001$ as determined by one-way ANOVA with multiple comparisons with a Tukey's post hoc test (**a**, **e**) or two-tailed Student's *t*-test (**f**). Data are represented as mean ± s.e.m.

novel function of HDAC3. Moreover, endogenous ERRα and HDAC3 co-immunoprecipitated in mature brown adipocytes (Extended Data Fig. 7c).

Inspection of the *Ucp1* locus revealed a super-enhancer (encompassing the eRNAs highlighted in Fig. 3b) at sites of co-localized HDAC3 and ERRα (Fig. 3g). Absence of HDAC3 led to marked attenuation of eRNA transcription and decreased levels of H3K27ac (Fig. 3g and Extended Data Fig 7d, e), along with pronounced reduction of *Ucp1* mRNA at 29 °C and 22 °C in both HDAC3 KO models (Fig. 3g and Extended Data Fig. 7f). Loss of HDAC3 had little or no effect on ERRα binding at the *Ucp1* locus (Fig. 3g and Extended Data Fig. 7g). Genetic ablation of ERRα decreased *Ucp1* expression and eRNA transcription in BAT (Extended Data Fig. 7h, i) as well as in mature brown adipocytes (Extended Data Fig. 7j), albeit to a lesser degree than HDAC3 KO perhaps because of redundancy with ERRγ[28]. These data strongly suggest that HDAC3 is a critical coactivator of ERR-driven thermogenic gene transcription in BAT.

Transcriptional activation by ERRα is highly dependent upon the coactivator peroxisome proliferator-activated receptor gamma coactivator 1 alpha (*Pgc-1α*, also known as *Ppargc1a*)[25,29]. Notably, the transcriptional function of PGC-1α is activated by lysine deacetylation[29], suggesting the possibility that HDAC3 may activate ERR-dependent transcription via deacetylation of PGC-1α. Indeed, HDAC3 markedly increased the transcriptional activity of ERRα at a major

HDAC3-bound enhancer of the *Ucp1* gene in the presence of WT PGC-1α but not a mutant form of PGC-1α that is unable to directly interact with ERRα (Fig. 4a). Both PGC-1α and HDAC3 co-immunoprecipitated with ERRα (Extended Data Fig. 8a), and HDAC3 robustly deacetylated PGC-1α that had been acetylated by the histone acetyltransferase GCN5 (ref. 29), both in cells and *in vitro*, and in a manner that was prevented by the class I HDAC inhibitor trichostatin A (Fig. 4b, c). HDAC3 also reversed GCN5-mediated repression of PGC-1α coactivator function (Extended Data Fig. 8b). Moreover, ectopic expression of non-acetylatable but not WT PGC-1α in primary brown adipocytes lacking HDAC3 (Extended Data Fig. 8c) markedly induced expression of *Ucp1* but not the adipocyte differentiation marker *Fasn* (Extended Data Fig. 8d).

In addition to the post-translational regulation of PGC-1α, the *Pgc-1α* genomic locus was bound by HDAC3 and ERRα at sites of potent enhancer activity that were lost in the absence of HDAC3 (Fig. 4d), and HDAC3 functioned as an activator at this enhancer (Fig. 4e). Indeed, *Pgc-1α* mRNA and protein were markedly reduced in HDAC3 KO BAT (Fig. 4f, g). Of note, combined deficiency of *Pgc-1α* and *Pgc-1β* (also known as *Ppargc1b*) leads to loss of BAT *Ucp1* expression and impaired mitochondrial function[30], reminiscent of the BAT HDAC3 KO phenotype. Enhancers at the gene encoding PGC-1β were also bound by HDAC3 and ERRα (Extended Data Fig. 9a), and *Pgc-1β* mRNA was markedly reduced in HDAC3 KO BAT (Extended Data Fig. 9b). Moreover, eRNAs at these sites were dependent upon HDAC3 (Extended Data Fig. 9c, d). Further, depletion of PGC-1α and β and/or ERRα in mature brown adipocytes decreased *Ucp1* transcription (Extended Data Fig. 9e). Thus, the ability of HDAC3 to activate PGC-1α both transcriptionally and post-translationally amplifies its coactivator function at ERR-family-regulated enhancers in a feed-forward manner (Fig. 4h).

Intriguingly, the transcription of *Ucp1* and *Pgc-1α* was even lower in the HDAC3 KO fat at thermoneutrality than at room temperature (Extended Data Fig. 9f), indicating that the effect of loss of HDAC3 on basal expression of these genes is more potent than eliminating sympathetic stimulation of BAT. This pattern of expression (HDAC3 KO < thermoneutrality < room temperature) was identified in many additional genes (Fig. 4i) critical for oxidative phosphorylation and energy metabolism (Fig. 4i, j). Thus, a critical function of HDAC3 in BAT is to maintain a minimal basal expression of *Ucp1* and other genes regulating energy metabolism.

The maintenance and protection of core body temperature through tight control of metabolism is a defining element of mammalian physiology. Our finding that BAT HDAC3 transcriptionally maintains the basal activity of thermogenic gene networks provides a physiological basis for the ability to rapidly generate heat in response to acute exposure to dangerously cold environmental temperatures. HDAC3 has a unique role in priming the brown adipocyte to support immediate thermogenic respiration and heat production without delay. Thus, distinct from adaptive (inducible) thermogenic mechanisms that require time to develop and respond, HDAC3 sets a basal thermogenic tone which establishes the facultative capacity of BAT to turn on rapidly, on-demand, to ensure readiness against acute and life-threatening cold exposure.

Online Content Methods, along with any additional Extended Data display items and Source Data, are available in the online version of the paper; references unique to these sections appear only in the online paper.

Received 20 July 2016; accepted 3 May 2017.
Published online 14 June 2017.

1. Cannon, B. & Nedergaard, J. Brown adipose tissue: function and physiological significance. *Physiol. Rev.* **84,** 277–359 (2004).
2. Guenther, M. G., Barak, O. & Lazar, M. A. The SMRT and N-CoR corepressors are activating cofactors for histone deacetylase 3. *Mol. Cell. Biol.* **21,** 6091–6101 (2001).
3. Chouchani, E. T. *et al.* Mitochondrial ROS regulate thermogenic energy expenditure and sulfenylation of UCP1. *Nature* **532,** 112–116 (2016).
4. Enerbäck, S. *et al.* Mice lacking mitochondrial uncoupling protein are cold-sensitive but not obese. *Nature* **387,** 90–94 (1997).
5. Ukropec, J., Anunciado, R. P., Ravussin, Y., Hulver, M. W. & Kozak, L. P. UCP1-independent thermogenesis in white adipose tissue of cold-acclimated *Ucp1*$^{-/-}$ mice. *J. Biol. Chem.* **281,** 31894–31908 (2006).
6. Bal, N. C. *et al.* Sarcolipin is a newly identified regulator of muscle-based thermogenesis in mammals. *Nat. Med.* **18,** 1575–1579 (2012).
7. Kazak, L. *et al.* A creatine-driven substrate cycle enhances energy expenditure and thermogenesis in beige fat. *Cell* **163,** 643–655 (2015).
8. Long, J. Z. *et al.* The secreted enzyme PM20D1 regulates lipidated amino acid uncouplers of mitochondria. *Cell* **166,** 424–435 (2016).
9. Harms, M. & Seale, P. Brown and beige fat: development, function and therapeutic potential. *Nat. Med.* **19,** 1252–1263 (2013).
10. Loft, A., Forss, I. & Mandrup, S. Genome-wide insights into the development and function of thermogenic adipocytes. *Trends Endocrinol. Metab.* **28,** 104–120 (2017).
11. Chen L.-f., Fischle, W., Verdin, E. & Greene, W. C. Duration of nuclear NF-kappaB action regulated by reversible acetylation. *Science* **293,** 1653–1657 (2001).
12. Bhaskara, S. *et al.* Deletion of histone deacetylase 3 reveals critical roles in S phase progression and DNA damage control. *Mol. Cell* **30,** 61–72 (2008).
13. Sun, Z. *et al.* Hepatic Hdac3 promotes gluconeogenesis by repressing lipid synthesis and sequestration. *Nat. Med.* **18,** 934–942 (2012).
14. Mullican, S. E. *et al.* Histone deacetylase 3 is an epigenomic brake in macrophage alternative activation. *Genes Dev.* **25,** 2480–2488 (2011).
15. Hoeksema, M. A. *et al.* Targeting macrophage histone deacetylase 3 stabilizes atherosclerotic lesions. *EMBO Mol. Med.* **6,** 1124–1132 (2014).
16. Razidlo, D. F. *et al.* Histone deacetylase 3 depletion in osteo/chondroprogenitor cells decreases bone density and increases marrow fat. *PLoS ONE* **5,** e11492 (2010).
17. Alenghat, T. *et al.* Histone deacetylase 3 coordinates commensal-bacteria-dependent intestinal homeostasis. *Nature* **504,** 153–157 (2013).
18. Montgomery, R. L. *et al.* Maintenance of cardiac energy metabolism by histone deacetylase 3 in mice. *J. Clin. Invest.* **118,** 3588–3597 (2008).
19. Sun, Z. *et al.* Diet-induced lethality due to deletion of the Hdac3 gene in heart and skeletal muscle. *J. Biol. Chem.* **286,** 33301–33309 (2011).
20. Rada-Iglesias, A. *et al.* A unique chromatin signature uncovers early developmental enhancers in humans. *Nature* **470,** 279–283 (2011).
21. Core, L. J., Waterfall, J. J. & Lis, J. T. Nascent RNA sequencing reveals widespread pausing and divergent initiation at human promoters. *Science* **322,** 1845–1848 (2008).
22. Fang, B. *et al.* Circadian enhancers coordinate multiple phases of rhythmic gene transcription *in vivo*. *Cell* **159,** 1140–1152 (2014).
23. Wang, D. *et al.* Reprogramming transcription by distinct classes of enhancers functionally defined by eRNA. *Nature* **474,** 390–394 (2011).
24. Gerhart-Hines, Z. *et al.* The nuclear receptor Rev-erbα controls circadian thermogenic plasticity. *Nature* **503,** 410–413 (2013).
25. Giguère, V. Transcriptional control of energy homeostasis by the estrogen-related receptors. *Endocr. Rev.* **29,** 677–696 (2008).
26. Soccio, R. E. *et al.* Genetic variation determines PPARγ function and anti-diabetic drug response *in vivo*. *Cell* **162,** 33–44 (2015).
27. Rajakumari, S. *et al.* EBF2 determines and maintains brown adipocyte identity. *Cell Metab.* **17,** 562–574 (2013).
28. Dixen, K. *et al.* ERRγ enhances UCP1 expression and fatty acid oxidation in brown adipocytes. *Obesity (Silver Spring)* **21,** 516–524 (2013).
29. Rodgers, J. T., Lerin, C., Gerhart-Hines, Z. & Puigserver, P. Metabolic adaptations through the PGC-1α and SIRT1 pathways. *FEBS Lett.* **582,** 46–53 (2008).
30. Uldry, M. *et al.* Complementary action of the PGC-1 coactivators in mitochondrial biogenesis and brown fat differentiation. *Cell Metab.* **3,** 333–341 (2006).

Supplementary Information is available in the online version of the paper.

Acknowledgements We thank the Next-Generation Sequencing Core and the Mouse Phenotyping, Physiology and Metabolism Core of the Penn Diabetes Research Center (National Institutes of Health (NIH) P30 DK19525). This work was supported by NIH R01 DK45586 (M.A.L.), NIH F30 DK104513 (M.J.E.), NIH R01 DK106027 (K.-J.W.), and the JPB Foundation.

Author Contributions M.J.E. and M.A.L. conceived the project, designed experiments, analysed results, and wrote the manuscript; M.J.E. performed animal experiments, immunoblots, RNA-seq, and ChIP–seq; M.J.E. and J.J. performed GRO-seq; H.-W.L. and K.-J.W. performed bioinformatic analyses; C.A.S. and M.J.E. performed mitochondrial assays. M.J.E. and H.J.R. performed cellular experiments. M.A. performed endogenous co-immunoprecipitation. D.J.S. performed H3/H3Kme1 ChIP–seq. L.C.P. and E.R.B. provided animal husbandry and technical assistance. T.M., Z.G.-H., P.S., J.A.B. and L.P. provided reagents and experimental design. All authors read and commented on the manuscript.

Author Information Reprints and permissions information is available at www.nature.com/reprints. The authors declare no competing financial interests. Readers are welcome to comment on the online version of the paper. Publisher's note: Springer Nature remains neutral with regard to jurisdictional claims in published maps and institutional affiliations. Correspondence and requests for materials should be addressed to M.A.L. (lazar@mail.med.upenn.edu).

Reviewer Information *Nature* thanks A. Vidal-Puig and the other anonymous reviewer(s) for their contribution to the peer review of this work.

METHODS

Statistical methods and reproducibility. Data are presented as mean ± s.e.m. unless otherwise stated. Graphpad Prism software was used for graphing and statistical analysis. All statistical tests are fully described in the figure legends and met criteria for normal distribution with similar variance. No statistical methods were used to pre-determine sample size. For comparison between two groups, a Student's *t*-test was used. For assessment between more than two groups, one-way ANOVA with multiple comparisons was used, and for assessment between two independent variables, two-way ANOVA with multiple comparisons was used, followed by a Tukey or Holm–Šidák post hoc test. For survival analysis, a log-rank (Mantel–Cox) test was performed. FDR for RNA-seq analysis was calculated by EdgeR bioinformatics software. Experiments independently repeated three or more times were Fig. 1a, b, 2b, 3c (ChIP), Fig. 3e (ChIP) and Fig. 4a, b, e, f and Extended Data Figs 1b, 3a–g, 7f, j, 8b and 9b, c. Experiments independently repeated two times were Fig. 1d, e and 4c, g and Extended Data Figs 1a, c–e, 2a–f, 5a, c–n, 7c, g and 8a, d. Experiments performed once were Figs 1c, 2a (RNA-seq), Fig. 3a, b (ChIP–seq, GRO-seq) Fig. 3c (ChIP–seq) and Fig. 3e (ChIP–seq) and Extended Data Figs 4b c, 5b, 6a–e, 7d–e, h–i and 9c, d.

Animal studies. Animal experiments were performed according to ethical regulations and protocols approved by the Institutional Animal Care and Use Committee of the Perelman School of Medicine at the University of Pennsylvania and the Children's Hospital of Philadelphia. All experiments used male age-matched littermates group housed at four or five animals per cage. Mice were group housed with enrichment in a temperature- and humidity-controlled, specific-pathogen free animal facility at 22 °C under a 12:12-h light:dark cycle with free access to standard chow (LabDiet, 5010) and water. High-fat diet studies were conducted by feeding mice a purified-ingredient diet composed of 60:20:20 kcal percentage of fat:carbohydrate:protein (Research Diets, D12492) at 12 weeks of age. Gene expression and protein studies were performed on 10- to 12-week-old male mice at zeitgeber time 10. Thermoneutrality and cold-exposure experiments were performed in climate-controlled rodent incubators (Powers Scientific) maintained at 29 °C or 4–5 °C, respectively, with interior temperature monitoring by digital thermometers. For thermoneutrality experiments, mice were allowed to acclimate to 29 °C for 2 weeks. No animals were excluded from studies and no randomization or blinding was performed.

HDAC3$^{loxP/loxP}$ mice maintained on a C57BL/6 background were bred to *Adipoq-cre*[31] mice maintained on a C57BL/6J background (The Jackson Laboratory, B6;FVB-Tg(Adipoq-Cre)1Evdr/J, Stock 010803), to *Ucp1-cre* mice maintained on a C57BL/6J background (The Jackson Laboratory, B6.FVB-Tg(Ucp1-Cre)1Evdr/J, Stock 024670), and to *Rosa26-CreER*^{T2} mice maintained on a C57BL/6J background (The Jackson Laboratory, B6.129-*Gt(Rosa)26Sor*$^{Tm1(cre/ERT2)Tyj}$/J, Stock 008463). *Ucp1*$^{-/+}$ mice maintained on a C57BL/6J background (The Jackson Laboratory, B6.129-Ucp1tm1Kz/J, Stock 003124) were used to generate *Ucp1*$^{-/-}$ and *Ucp1*$^{+/+}$ mice. ERRα$^{-/+}$ (also known as *Esrra*$^{-/+}$) mice maintained on a C57BL/6 background were used to generate ERRα$^{-/-}$ and ERRα$^{+/+}$ mice as previously described[32]. Tissue-specific HDAC3 KO mice were generated by mating males heterozygous for *Adipoq-cre* or *Ucp1-cre* and homozygous for the floxed HDAC3 alelle to females homozygous for the HDAC3 allele. Male littermate Cre-positive (HDAC3 KO) and Cre-negative (littermate controls) mice were then group housed upon weaning.

Core body temperature measurements and cold-tolerance testing. Baseline measurements of internal core body temperatures were recorded from 10-week-old male mice maintained at 22 °C (starting at zeitgeber time 4) using a digital thermometer (Oakton Instruments, Temp 10T Thermocouple) and rectal thermocouple probe (Physitemp, RET-3 probe). Cold-exposure studies were performed within climate-controlled rodent incubators. Mice were placed in pre-chilled cages at 4–5 °C with bedding, a cotton nestlet, free access to standard chow and water, and cage lid partly open. Rectal temperatures were recorded every 60 min. Individual mice were removed from the study and euthanized if core body temperature fell ≥10 °C from baseline measurement. Core temperatures ≥10 °C from baseline measurement were not included in core temperature analysis and scored as an event for survival analysis.

Whole-animal oxygen consumption rate. Oxygen consumption rates of 10-week-old male mice were measured using Comprehensive Laboratory Animal Monitoring System (CLAMS, Columbus Instruments) metabolic cages housed within environment-controlled rodent incubators. Following previously described protocols[33], mice maintained at 22 °C were anaesthetized with 75 mg per kg (body weight) pentobarbital (Nembutal) by intraperitoneal injection and placed into CLAMS cages pre-acclimated to 33 °C to maintain mouse body temperature while under anaesthesia. Before noradrenaline-induced oxygen consumption readings, baseline oxygen consumption measurements were recorded for several cycles after pentobarbital administration until stable readings were recorded. A subcutaneous injection of 1 mg per kg (body weight) L-(−)-noradrenaline (+)-bitartrate salt monohydrate (Sigma, A9512) dissolved in sterile 0.9% NaCl (Sigma, S8776) was given into the dorsal nuchal region. After injection, individual mice were immediately placed into the CLAMS cages and oxygen consumption rates were recorded until rates began to decline.

***In vivo* metabolic phenotyping.** Whole-body energy metabolism was evaluated using a CLAMS. Mice were singly housed and acclimated in metabolic chambers for 48 h before data collection. Each mouse was continuously monitored for physical activity and food intake. CO_2/O_2 levels were collected four or five times per hour per mouse over the duration of the experiment. Analysis of covariance (ANCOVA) of VO_2 versus body mass during light, dark, and 24 h periods was performed through the NIDDK Mouse Metabolic Phenotyping Centers Energy Expenditure Analysis website (http://www.mmpc.org/shared/regression.aspx). Body composition analyses by NMR were performed using Echo-MRI (Echo Medical Systems) to measure fat and lean mass.

BAT mitochondrial respiration assays. Mitochondrial respiration rates were determined using an O2K high-resolution respirometer (Oroboros Instruments, Austria). To preserve all populations of mitochondria, whole-tissue homogenates were prepared from BAT minced on ice and dounced at 4 °C (150 r.p.m. × eight strokes) in 15 ml of ice-cold mitochondrial isolation buffer (210 mM mannitol, 70 mM sucrose, 10 mM HEPES, 1 mM EGTA, adjusted to pH 7.2 with KOH)[34–36]. Homogenates were centrifuged at 8,500*g* for 10 min at 4 °C. Lipid and supernatant were discarded. Pellet was re-suspended in 1 ml of ice-cold mitochondrial isolation buffer, passively filtered (100 μm), and protein concentration determined by BCA assay.

Respirometry measurements were performed using homogenates (0.25 mg) re-suspended in respiration buffer and maintained at 37 °C (110 mM mannitol, 0.5 mM EGTA, 3 mM $MgCl_2$, 20 mM taurine, 10 mM KH_2PO_4, 60 mM K lactobionate, 0.3 mM DTT, and 0.1% BSA (fatty acid free), adjusted to pH 7.1). Samples were vigorously stirred by magnetic stir bar and the O_2 concentration maintained between 100 and 200 nmol ml^{-1}. UCP1-dependent respiration and individual complex-dependent respiration rates were determined by a standard substrate/inhibitor titration protocol. After stabilization, real-time oxygen concentration and flux data were collected continuously (DatLab software 4.3, Oroboros Instruments, Austria). Baseline respiration following the addition of substrate (palmatoylcarnitine (4 mM), pyruvate (10 mM), and malate (5 mM)) was measured. UCP1-dependent respiration was assessed by addition of 2 mM guanosine diphosphate. Independent complex-dependent respiration was then determined in the presence of ADP (1 mM). To assess complex-II-dependent respiration, rotenone (0.5 μM) was added to selectively inhibit complex I followed by succinate (10 mM), a complex II substrate. Antimycin A (5 μM) was then added to inhibit complex III followed by addition of TMPD (0.5 mM) and ascorbate (2 mM) as artificial electron donors for complex IV. Sodium azide (2.5 mM) was used to assess the contribution of leak respiration independent of complex IV[37,38].

Histological analysis. Adipose tissues were fixed in 4% paraformaldehyde/1× PBS overnight at 4 °C and dehydrated through sequential ethanol washes. Tissue was embedded in paraffin before sectioning and then stained with haematoxylin and eosin. Stained sections were visualized and photographed under bright-field microscopy.

RNA isolation and gene expression analysis (RT–qPCR). Total RNA was isolated from snap-frozen adipose tissues, which were mechanically homogenized in 500 μl TRIzol (Life Technologies) in a TissueLyser (Qiagen) for 5 min, at a frequency of 20 s^{-1}. After homogenization, samples were centrifuged at 4 °C and homogenates transferred to a fresh tube for RNA extraction with chloroform. Aqueous chloroform fractions were mixed with equal volumes of 70% ethanol/30% water and RNA further purified with RNeasy Mini spin columns (Qiagen) and on-column DNase-digestion (Qiagen). TRIzol phases were saved for further isolation of genomic and mitochondrial DNA. One and a half micrograms of total RNA was used for complementary DNA synthesis using a High-Capacity cDNA Reverse Transcription kit (Applied Biosystems). Complementary DNAs (cDNAs) were analysed by qPCR using a Power SYBR Green PCR Master mix on a Quant Studio 6 Flex Real-Time PCR system (Applied Biosystems). All qPCR data were analysed using a standard curve and normalized to *36B4* (also known as *Arbp*) or *18S* expression. Specific primer sequences are listed in a primer table in the Supplementary Information.

Quantification of mitochondrial content. Total DNA was precipitated from TRIzol tissue extraction by ethanol precipitation and centrifugation, followed by sodium citrate/ethanol solution (0.1 M sodium citrate/10% ethanol, pH 8.5) washes of DNA pellet. DNA pellet was allowed to air dry before re-suspension. DNA samples were analysed by qPCR using a standard curve to determine absolute mitochondrial DNA abundance normalized to nuclear genomic DNA abundance. Specific primer sequences are listed in a primer table in the Supplementary Information.

Immunoblotting. Interscapular BAT samples were homogenized in radioimmunoprecipitation assay buffer (150 mM NaCl, 1.0% NP-40, 0.5% sodium deoxycholate, 0.1% SDS, 50 mM Tris-HCl pH 8.0, 5 mM EDTA, 5 mM NaF, 1 mM Na_3VO_4) with 1 mM phenylmethylsulfonylfluoride, supplemented with complete protease inhibitor (Roche), using a TissueLyser (Qiagen) for 3 min at a frequency of 20 s^{-1} at 4 °C followed by sonication with a Biorupter (Diagenode) for 30 s. For nuclear extracts, nuclei were prepared by dounce homogenization of five frozen BAT pads thawed in swelling buffer plus protease inhibitor (10 mM Tris-HCl, 2 mM $MgCl_2$, 3 mM $CaCl_2$), dounced with pestle A/B, filtered with 100 μm cell strainer, pelleted at 600*g*, and re-suspended in swelling buffer with cells lysed in an equal volume of lysis buffer (swelling buffer + 10% glycerol + 1% NP-40). Nuclei were isolated by centrifugation at 600*g* and soluble protein extracted by re-suspending in 4 pellet volumes of modified nuclear extract buffer (20 mM HEPES, 0.42 M KCl, 3 mM $MgCl_2$, 10% glycerol, 3 mM 2-mercaptoethanol, 0.5% Trition-X, 1 mM EDTA, and 1 mM EGTA) plus protease inhibitors and incubated at 4 °C with rotation for 2 h. Protein concentration was determined using a Direct Detect Spectrometer (EMD Millipore) and protein loaded onto 10% Criterion TGX gels (Bio-Rad) by SDS–polyacrylamide gel electrophoresis, and transferred to a polyvinylidene difluoride (PVDF) membrane. After antibody incubation, immunoblots were visualized using enhanced chemiluminescence substrates (Western Lightning Plus-ECL, PerkinElmer; or SuperSignal West Dura, Thermo) by autoradiography film or Bio-Rad ChemiDoc Imaging.

Antibodies. The following antibodies were used for western blotting: HDAC3 (GeneTex, GTX113303, Lot 40436), HDAC3 (Abcam, 76295), β-actin (Abcam, 8226) (Abcam, 20272), ERRα (Abcam, 16363), HSP90 (Cell Signaling, 4874), vinculin (Sigma, V9264), acetylated lysine rabbit polyclonal (Cell Signaling, 9441, Lot 12), UCP1 (R&D, MAB6158), HA tag (GeneTex, 115044-01), Myc tag (GeneTex, 21261), V5 tag (ThermoFisher, R960-25), Pol II antibody (N-20, Santa Cruz 899 X, Lot K1215), GCN5 (H-75, Santa Cruz 20698, Lot K0112), PGC-1α mouse monoclonal antibody (EMD Millipore, 4C.13, ST1202, Lot TE0349482), anti-rabbit IgG-HRP (Cell Signaling, 7074), anti-mouse IgG-HRP (Cell Signaling, 7076), mouse monoclonal SB62a anti-rabbit IgG light chain (HRP) (Abcam, 99697). The following antibodies were used for ChIP: HDAC3 (Abcam, 7030, Lot GR121157-6), H3K27ac (Abcam, 4729, Lot GR251958-1), ERRα (Abcam, 16363, Lot GR263385-1), NCoR (previously described[39], raised in rabbit against amino acids 1944–2453, affinity purified), H3K4me1 (Abcam, 8895), and H3 (Abcam, 1791).

Cell culture. NIH/3T3 cells (ATCC, CRL1658) were maintained at 37 °C in 5% CO_2 in high-glucose Dulbecco's modified Eagle's medium (DMEM) supplemented with 10% bovine calf serum (Sigma) and 1% penicillin–streptomycin (Gibco); HEK-293FT cells (Thermo, R700-07) were maintained at 37 °C in 5% CO_2 in high-glucose DMEM supplemented with 10% fetal bovine serum (Tissue Culture Biologicals) and 1% penicillin–streptomycin (Gibco). All lines were passaged at approximately 80–85% confluence. Immortalized brown pre-adipocytes[40] were maintained at 37 °C in 5% CO_2 in DMEM/F-12 Glutamax, 10% FBS, 1% penicillin–streptomycin (Gibco). NIH/3T3 and HEK-293FT cell lines were low passage and not tested for mycoplasma. Immortalized brown pre-adipocytes tested negative for mycoplasma using a MycoAlert Mycoplasma Detection kit (Lonza).

Primary brown adipocyte isolation and differentiation. Matings of *Rosa26-CreER*-positive, $Hdac3^{f/f} \times Hdac3^{f/f}$ mice were used to generate *Rosa26-CreER*-postive, $Hdac3^{f/f}$, and littermate control $Hdac3^{f/f}$ pups. Pre-adipocytes were isolated from BAT depots of postnatal day 1–3 mice and tails saved for genotyping. Individual depots were placed into 200 μl DMEM/F-12 Glutamax (Invitrogen) and minced finely with spring scissors (Roboz) before digestion in 1 ml 1.5 U ml^{-1} collagenase D (Roche) and 2.4 U ml^{-1} Dispase II (Roche) at 37 °C in a thermocycler for 40 min at 1,200 r.p.m. Cells were purified through 100 μm filters (Millipore) into 5 ml of DMEM/F-12 Glutamax with 10% FBS, pelleted at 700*g*, and re-suspended in growth media (DMEM/F-12 Glutamax, 10% FBS, 1% penicillin–streptomycin (Gibco), and primocin (Invivogen)). Pre-adipocytes of the same genotype were pooled, re-plated, and, upon confluence, adipocyte differentiation was initiated with induction media (growth media supplemented with 500 nM dexamethasone, 125 μM indomethacin, 0.5 mM IBMX, 1 μM Rosi, 1 nM T3, 20 nM insulin) for 48 h. After induction, cells were cultured in maintenance media (growth media plus 1 nM T3, 20 nM insulin) and media refreshed every 48 h. For inducible HDAC3 deletion experiments, 2 μM 4-hydroxytamoxifen (Sigma) was added to induction media of both *Rosa26-CreER*-positive and *Rosa26-CreER*-negative cells from days 0 to 2. All analysis was performed on day 8 cultured brown adipocytes.

Retrovirus. WT *Pgc-1α* DNA and a non-acetylatable *Pgc-1α* mutant (R13) cDNA were cloned into a murine stem cell virus (MSCV) retroviral construct. Retrovirus was produced in HEK-293FT cells by co-transfection of MSCV and pCL-Eco vectors with FuGENE 6 (Promega), and supernatants were harvested 72 h after transfection. Supernatants were passed through a 0.20 μm filter (Corning) before viral concentration with PEG-it Virus Precipitation Solution (System Biosciences) at 4 °C. Twenty-four-well plates were seeded with 6×10^4 brown pre-adipocytes per well and MSCV retroviruses were added upon cell adherence in media containing 2 μg ml^{-1} polybrene and allowed to reach confluence before adipocyte differentiation.

Dual luciferase assays. The mouse *Ucp1* (−6 k) enhancer (389 base pairs (bp)) containing ERRα and HDAC3 binding sites, was PCR-amplified from C57BL/6 genomic DNA using primers listed in a primer table in the Supplementary Information to add XhoI and BglII sites for cloning into the pGL4.24 luciferase vector (Promega). The mouse *Pgc-1α* (−38 k) enhancer (998 bp) containing identified binding sites was PCR-amplified from C57BL/6 genomic DNA using the primers listed in the table in Supplementary Information and Gibson cloned between the NheI and BglII sites of the pGL4.24 luciferase vector. Luciferase assays were performed by transient transfection of NIH/3T3 cells seeded at a density of 1.25×10^5 cells per well (24-well plate) using Lipofectamine 2000 (3:1 ratio, Lipofectamine:DNA). Optimized transfections were performed using 1,200 ng DNA to 500 ng pGL4.24 luciferase vector and 2.0 ng Renilla luciferase (for normalization) plus factor expression vectors and/or empty pcDNA3.1. Twenty-four hours after transfection, cell lysates were harvested using a Dual Luciferase kit (Promega) to measure luciferase activities on a Synergy HT plate reader (Biotek).

Immunoprecipitation assays. For cellular acetylation experiments, HEK-293FT cells were co-transfected with combinations of pcDNA3.1-GFP, pcDNA3.1-HA-PGC-1α, pcDNA3.1-HDAC3-myc, pcDNA3.1-Flag-GCN5, and/or empty pcDNA3.1. Forty-eight hours after transfection, cells were harvested in ice-cold NP40 IP lysis buffer (20 mM Tris-HCl, 150 mM NaCl, 10% glycerol, 2 mM EDTA, 0.1% NP40, 10 mM NaF, with 1 mM DTT, 1 mM phenylmethylsulfonylfluoride), and supplemented with complete protease inhibitor cocktail (Roche), 4 μM trichostatin A (Cell Signaling), 5 mM nicotinamide (Sigma), and 1 μM bortezomib (Cell Signaling) on ice. Cell lysates were freeze/thawed in liquid nitrogen twice, and lysates cleared by centrifugation at 4 °C for 10 min. Two hundred and fifty milligrams of protein was used for each immunoprecipitation and the volume adjusted to 1 ml with lysis buffer. Washed anti-haemagglutinin (HA) agarose beads (Pierce) were incubated with samples and rotation at 4 °C for 4 h, followed by three brief washes with lysis buffer. Immunoprecipitated proteins were eluted in 2× loading buffer with boiling at 95 °C for 5 min.

Co-immunoprecipitation. For endogenous co-immunoprecipitations, protein lysates were made from day 8 differentiated brown adipocytes in IPLS buffer (50 mM Tris-HCl pH7.4, 150 mM NaCl, 0.5% NP-40) with protease and phosphatase inhibitor (Roche). Lysates were sonicated, lipid removed by centrifugation at 4 °C, and 0.5 mg protein lysate was pre-cleared with anti-rabbit Trueblot beads (Rockland) for 3 h at 4 °C with rotation. One per cent of total pre-cleared lysate was saved for input. Pre-cleared lysate was then incubated with anti-HDAC3 (Abcam, 7030) at 4 °C for 2 h with rotation, followed by immunoprecipitation with conjugated anti-rabbit goat IgG Trueblot beads for 1 h at 4 °C. Beads were washed four times with IPLS buffer plus inhibitors and samples eluted in 2× loading buffer at 55 °C for 20 min with agitation, supernatant isolated from beads, 2-mercaptoethanol (BME) and 1,3-dithiothreitol (DTT) added, and boiled at 95 °C for 5 min. Eluted proteins were resolved by immunoblotting and PVDF membrane incubated with anti-ERRα (Abcam, 16363) overnight at 4 °C, a conformation-specific secondary mouse anti-rabbit IgG-HRP, and then developed. The blot was stripped (Restore Plus, Thermo), blocked, and incubated overnight at 4 °C with HDAC3 (Abcam, 76295) followed by incubation with conformation-specific secondary mouse anti-rabbit-HRP. For overexpression co-immunoprecipitation experiments, V5-tagged ERRα and/or HA-tagged PGC-1α and myc-tagged HDAC3 were co-transfected into HEK-293FT cells for 48 h. Forty-eight hours after transfection, cells were harvested in ice-cold IPLS buffer supplemented with complete protease inhibitor cocktail, 1 mM phenylmethylsulfonylfluoride, and 1 μM bortezomib on ice. Cell lysates were freeze/thawed in liquid nitrogen twice, sonicated, and lysates cleared by centrifugation at 4 °C for 10 min. One hundred milligrams of lysate was pre-cleared with Mouse IgG Sepharose Bead Conjugate (Cell Signaling, 3420) before immunoprecipitation with V5-agarose beads (Sigma, A7345) at 4 °C for 2 h. Beads were washed four times in IPLS buffer and eluted in 2× loading buffer at 95 °C for 5 min, the supernatant isolated from the beads, and BME added and boiled at 95 °C for 5 min. Immunoblot for myc-HDAC3 was performed using goat anti-myc HRP (GeneTex), stripped, re-developed, and then immunoblotted for V5-ERRα with mouse monoclonal anti-V5 (ThermoFisher).

Protein purification. HA-tagged PGC-1α was co-transfected into HEK-293FT cells with GCN5 for 48 h and the cells were lysed in radioimmunoprecipitation assay lysis buffer supplemented with complete protease inhibitor cocktail (Roche), 1 mM phenylmethylsulfonylfluoride, 4 μM trichostatin A (Cell Signaling), 5 mM nicotinamide, and 1 μM bortezomib (Cell Signaling) on ice. Lysate was sonicated, cleared by centrifugation, and immunoprecipitation of acetylated PGC-1α performed with anti-HA agarose beads (Pierce) at 4 °C with rotation in the presence of inhibitors. Sequential washes (with inhibitors) were performed: six

washes with radioimmunoprecipitation assay buffer, two washes with high salt wash buffer (10 mM Tris-HCl pH 8.0, 250 mM LiCl, 0.5% NP-40, 0.5% sodium deoxycholate, 1 mM EDTA), followed by two washes in 1× PBS. The purified protein remained immobilized on HA-beads in the presence of inhibitors before deacetylation assay.

***In vitro* deacetylation assay.** Immobilized pre-acetylated PGC-1α was washed three times with HDAC assay buffer (Enzo). Thirty microlitres of the bead slurry was added to 100 μl HDAC assay buffer containing buffer alone, 100 ng recombinant human HDAC3/NCoR-DAD (Enzo), or 100 ng recombinant human HDAC3/NCoR-DAD plus 4 μM trichostatin A, and incubated at 37 °C with agitation for 1 h. After the reaction, the beads were boiled in 2× loading buffer with BME at 95 °C and acetylation of PGC-1α was assessed by western blot.

Acute siRNA knockdown in immortalized brown adipocytes. Acute siRNA knockdown was performed via reverse-transfection. Sixty thousand differentiated brown adipocytes (day 5) were seeded into 96-well plates containing Lipofectamine RNAiMax and siRNAs (pre-incubated for 25 min in wells) or into no transfection control. Total RNAi concentration was held constant at 50 nM. Seventy-two hours after transfection, day 8 brown adipocytes were harvested in TRIzol for analysis by RT–qPCR. ON-Target Plus SMARTpool siRNAs targeting mouse *ERRα* (Dharmacon, L-040772-00, target sequence 5′-GCUGAAAGCUCUGGCCCUU-3′, 5′-GCGGAGGACGGCAGAAGUA-3′, 5′-CUGAGAAGCUGUACGCCAU-3′, 5′-GCAUCGAGCCUCUCUACAU-3′), *Ppargc1a* (Dharmacon, L-040773-01, 5′-GAACAAGACUAUUGAGCGA, 5′-UUACGCAGGUCGAACGAAA-3′, 5′-ACAAUGAGCCUGCGAACAU-3′, 5′-CAGCCGAGGACACGAGGAA-3′), *Ppargc1b* (Dharmacon, L-040905-01, 5′-UGGUACAGCUCAUUCGCUA-3′, 5′-GGGAAAAGCAAGUACGAAG-3′, 5′-GCUUUGAGGUGUUCGGUGA-3′, 5′-GGAAAAGGCCAUCGGUGAA-3′) or non-targeting control (Dharmacon, D-001810-10, 5′-UGGUUUACAUGUCGACUAA-3′, 5′-UGGUUUACAUGUUGUGUGA-3′, 5′-UGGUUUACAUGUUUUCUGA-3′, 5′-UGGUUUACAUGUUUUCCUA-3′) were used.

RNA-seq library preparation. Total RNA was extracted from interscapular BAT pads of 12-week-old male mice adapted to thermoneutrality for 2 weeks. One microgram of purified DNase-treated total RNA from biological replicates (four WT control *Hdac3*$^{f/f}$, four KO *Adipoq-cre*; *Hdac3*$^{f/f}$) was processed with a Ribo-Zero Magnetic rRNA removal kit (Epicentre, MRZH11124). The RNA libraries were prepared using a TruSeq RNA Sample Prep kit v2 (Illumina, RS-122-2001) and standard Illumina protocol. RNA-seq libraries were sequenced at single-end 100 bp read length on an Illumina HiSeq 2000.

RNA-seq data analysis. RNA-seq reads were aligned to the University of California, Santa Cruz (UCSC) mm9 genome browser using TopHat2 (ref. 41). For differential gene expression analysis, raw read counts were measured within RefSeq genes using featureCounts[42], and an exact test was performed using the edgeR pipeline[43]. Genes were included in differential expression analysis if their expression levels were >0.5 RPKM in at least three samples. Genes having a fold change of >1.5 (either up or down) and FDR of <0.01 were selected as HDAC3-KO-regulated genes. Gene Ontology analysis was performed used Enrichr[44,45], where the top-ranked KEGG pathway, Biological Process, and Cell Component terms were selected by Enrichr combined score. Representative downregulated genes identified by Gene Ontology were presented with their $\log_2$(fold change) as a heat map. As an extended figure, all TCA cycle and mitochondrial respiratory chain complex genes retrieved from the HUGO gene nomenclature database[46] were presented by heat map to show quantitative trends identified in Gene Ontology. For genome browser visualization, bigwig files[47] were generated for individual replicates in a 1-bp-resolution RPM scale using genomeCoverageBed with '-split' option in bedtools[48] and bedGraphToBigWig in the SRA toolkit[49]. A representative track was generated for each condition from the replicate bigwig files. All the genome browser snapshots were taken via IGV[50,51].

ChIP. HDAC3 ChIP was performed as previously described[14,39] with modification. Immediately after euthanasia, the entire interscapular BAT pad (two lobes) was snap-frozen. Tissue was later thawed and minced directly in cross-linking solution (10 ml, 1× PBS/1% formaldehyde) and allowed to rock for 20 min at room temperature. For epididymal white adipose tissue (eWAT) ChIP, two fat pads per mouse were processed in an identical fashion to BAT. Cross-linking was quenched by addition of 0.5 ml of 2.5 M glycine and allowed to mix for 5 min, followed by three ice-cold 1× PBS washes. Cross-linked tissue pieces were re-suspended in ice-cold ChIP dilution buffer (50 mM HEPES pH7.5, 155 mM NaCl, 1 mM EDTA, 1.1% Triton X-100, 0.11% sodium deoxycholate, 0.1% SDS) with protease inhibitors (cOmplete Protease Inhibitor, Roche) and placed on ice. Chromatin fragmentation was performed using probe sonication at 4 °C (Fischer Scientific, FB705 Sonic Dismembrator) for three cycles of 10 s at 10% amplitude, followed by three cycles of 10 s at 15% amplitude, with a 30 s pause on ice between cycles. Chromatin lysates were cleared of lipid by centrifugation at 4 °C. Chromatin lysates were brought to 1 ml with ChIP dilution buffer, input saved, and incubated with antibodies overnight at 4 °C, then immunoprecipitated with BSA blocked Protein A Sepharose CL-4B Beads (GE Healthcare) with rotation for 2 h at 4 °C. Immunoprecipitations were washed: one quick wash 1 ml ChIP dilution buffer, one 5 min wash ChIP dilution buffer, one 5 min wash in 1 ml ChIP dilution buffer with 500 mM NaCl, one 5 min wash in ChIP wash buffer (10 mM Tris-HCl pH 8.0, 250 mM LiCl, 0.5% NP-40, 0.5% sodium deoxycholate, 1 mM EDTA), followed by one 5 min wash in Tris-EDTA (10 mM Tris-HCl pH 8.0, 1 mM EDTA). Cross-linking was reversed overnight at 65 °C in elution buffer (50 mM Tris-HCl pH 8.0, 10 mM EDTA, 1% SDS), removed from beads, incubated with proteinase K, and DNA was isolated using phenol/chloroform extraction in 2 ml Phase Lock Gel tubes (5 Prime) followed by NaCl/EtOH-mediated DNA precipitation overnight at −20 °C with 20 μg glycogen carrier (Roche).

ChIP–seq library preparation. For BAT ChIP–seq of HDAC3, ERRα, and NCoR, five biological replicate ChIPs were pooled for sequencing. For BAT ChIP–seq of H3K27ac, replicate ChIPs were pooled into two libraries (three samples per library) for sequencing and library reads pooled into one dataset. Enzymes from New England Biolabs were used to generate libraries according to the ChIP Sequencing Sample Preparation Guide provided by Illumina. Adaptor oligonucleotides and primer sequences from Illumina were used for library construction and amplification. Before PCR library amplification, size selection of adaptor-ligated DNA was performed using Agencourt AMPure XP Beads (Beckman Coulter). PCR Purification and MinElute (Qiagen) kits were used for library purification steps.

ChIP–seq data analysis. All ChIP–seq libraries were sequenced on HiSeq 2500 (single-end 50 bp or 100 bp) or NextSeq 500 (single-end 75 bp or 76 bp) systems. Before alignment, all reads were adjusted to 50 bp by trimming the 3′ end to avoid any bias due to different read lengths. Sequencing reads were aligned to the UCSC mm9 using Bowtie[52]. All peak calling was performed with the findPeaks command in the Homer package[53]. For HDAC3 peak calling, WT and HDAC3-KO aligned reads were down-sampled to 20 million reads to adjust read-depth bias and avoid peak saturation, and duplicate reads were removed except for one. Stringent HDAC3 peaks were called in the WT sample against the KO sample using option '-F 3' (FDR < 0.001). ERRα peaks in WT and HDAC3-KO mice and NCoR peaks in WT mice were called against an input using default options (FDR < 0.001). After initial peak calling, all peaks were resized into 200 bp followed by 1 RPM cutoff, and peaks within the ENCODE blacklist regions[54] were discarded. When visualizing HDAC3, ERRα, and NCoR ChIP–seq profiles (line plots and heat maps), we used control-subtracted signal: KO sample for HDAC3, input sample for ERRα and NCoR. All bigwig files were generated using Homer and the bedGraphToBigWig command. HDAC3 and ERRα ChIP–seq signals were compared by RPM-normalized tag counts between KO-repressed and unchanged eRNAs within a 400 bp window, where the *P* value was calculated by a Wilcoxon test.

Two biological replicates of H3K27ac ChIP–seq were prepared from both WT and HDAC3-KO BAT. Duplicate reads were condensed and replicates were pooled for visualization in a genome browser. H3K27ac levels at HDAC3-bound enhancer nearby KO-regulated genes were compared between WT and KO mice by RPM-normalized tag counts within a 2 kb window around HDAC3 peaks, and *P* values were calculated by a Wilcoxon test. Super-enhancers were called on the basis of the H3K27ac data using a ROSE pipeline with default options. H3K4me1 and H3 ChIP–seq data in WT BAT and WT eWAT were generated to prepare an eRNA filter for GRO-seq analysis. Together with previously published adipose H3K27ac data[55] (GSE63964), histone modification peaks were called against corresponding H3 ChIP–seq samples in each depot by Homer with an option '-style histone -F 3' (FDR <0.001).

De novo motif searches of ChIP–seq peaks were performed using the findMotifsGenome command in Homer within a 200 bp window with default options. Discovered motifs were ranked by *P* values calculated on the basis of a binomial test against GC%-matched background, and the top four motifs presented.

GRO-seq library preparation. GRO-seq was performed and analysed as previously described[22], with minor modifications for mouse interscapular BAT samples. Ten interscapular BAT pads from genotype-confirmed *Adipoq-cre*, HDAC3 KO, and control littermates were quickly dissected, immediately pooled and minced in ice-cold nuclei isolation buffer A, and dounce homogenized on ice to isolate ~40 million nuclei. Aliquots of nuclei preparations were inspected visually for quality under a microscope with DAPI (4′,6-diamidino-2-phenylindole) staining, and nuclei counted using a Countess Automated Cell Counter (Invitrogen). The nuclear run-on reaction was performed for 7 min and RNA hydrolysis was allowed to proceed for 10 min. All GRO-seq library preparations were performed in parallel to avoid batch effects.

GRO-seq data analysis. Before alignment, sequencing reads were cleaned by trimming off low-quality base, adaptor, and poly-A tailing sequences using cutadapt[56]. Trimmed reads of at least 25 bp were selected and aligned to UCSC mm9 using Bowtie[52] with an option '––best ––strata -m 1 -v 3'. Aligned reads within extremely high signal regions (such as ribosomal RNA, small nucleolar RNA, small nuclear

RNA, and transfer RNA) were removed before downstream analysis to minimize read-depth bias. For genome browser visualization, bigwig files were generated separately for (+) and (−) strands, and all reads were extended to 150 bp for smooth profile. All (−) strand signals were presented as negative values.

Gene body transcription levels were quantitated in all conditions for comparative analysis. First, all reads were extended to 50 bp towards the 3′ end, then RPKM-normalized read counts were measured within RefSeq gene bodies excluding the 500 bp region at the 5′ end. However, for genes with total gene length <1 kb, the entire gene body was used. Gene transcription levels were further normalized among conditions for global bias correction using loess normalization in the limma package[57]. A gene was classified as 'transcribed' in a given condition if the transcription level was >0.3 RPKM. Genes that were not transcribed throughout all conditions were eliminated before downstream analysis. A gene was defined as 'differential' between a given pair of conditions if it was transcribed in either condition and the fold change was greater than 1.5 (either up or down). *Ucp1* and *Ppargc1a* nascent transcription levels were compared between genotypes and between temperatures via an exact test in EdgeR[43,58] using a common dispersion estimated from housekeeping genes.

Hierarchical clustering was performed for nascent gene transcription level at 22 °C and 29 °C in WT and HDAC3 KO mice to identify an HDAC3-dependent functional module. First, putatively highly variable genes were selected by fold change >1.5 between maximum and minimum transcription levels. Next, clustering was done for $\log_2$-transformed gene transcription level by Ward's criterion using a Pearson correlation coefficient as a similarity measure. One cluster of genes was identified that displayed similar transcriptional changes to *Ucp1* or *Ppargc1a* genes. Overall gene transcription trend was visualized as a box plot in *z*-score scale. Next, Gene Ontology analysis was performed for this cluster using Enrichr; top-ranked Biological Process terms and KEGG pathways were selected and their relative gene transcription levels were visualized by a heat map in *z*-score scale.

eRNA calling was performed as previously described[22,59] with minor optimization. First, eRNA peaks were called separately on each strand for all samples via Homer peak calling using the option '-style factor -separate -center -fragLength 150 -size 200 -minDist 400 -tbp 0 -L 3 -localSize 10000 -fdr 0.001'. Next, another round of peak calling was performed using the same option for intergenic reads only to rescue promoter-proximal eRNA peaks skipped by local background effect of highly transcribed genes. All eRNA peaks, excluding those falling into TSS 2kb and TTS 2kb windows, were then pooled and merged among biological conditions to prepare a master eRNA peak set. Next, a series of filters was applied: (1) peaks within ENCODE blacklist regions were discarded; (2) small peaks (<0.2 RPM) or any peaks embedded within same-stranded gene transcription were discarded; (3) an epigenomic filter was applied using active enhancer marks, H3K27ac and H3K4me1 from BAT and eWAT, to broadly define and capture adipose eRNAs. Remaining peaks were then paired between opposite strands if their distance was <1 kb. For paired eRNA peaks, their centre was defined as an enhancer; for unpaired eRNA peaks, their 5′ upstream 180 bp positions were defined as enhancers.

eRNA transcription levels were measured in RPKM within a 1 kb window around enhancers. If an enhancer was intergenic, both strands were measured; if it was within a transcribed gene body, only the anti-sense signal was measured. After measuring eRNA levels in all conditions, loess normalization was applied for global bias correction as previously performed in the gene transcription analysis. For differential analysis comparing two different conditions, eRNAs with >0.5 RPKM in at least one condition were selected, then eRNAs with a fold change >2 (either up or down) were defined as differential eRNAs. *De novo* motif search for eRNAs was performed within a 400 bp window using Homer, and the top four motifs selected by *P* value were presented.

Data availability. All ChIP–seq, RNA-seq, and GRO-seq data reported here have been deposited in the Gene Expression Omnibus under accession number GSE83928. Source Data and uncropped gels for figures are provided with the online version of the paper. Data that support the findings of this study are available from the corresponding author upon reasonable request.

31. Mullican, S. E. *et al.* A novel adipose-specific gene deletion model demonstrates potential pitfalls of existing methods. *Mol. Endocrinol.* **27,** 127–134 (2013).
32. Luo, J. *et al.* Reduced fat mass in mice lacking orphan nuclear receptor estrogen-related receptor α. *Mol. Cell. Biol.* **23,** 7947–7956 (2003).
33. Cannon, B. & Nedergaard, J. Nonshivering thermogenesis and its adequate measurement in metabolic studies. *J. Exp. Biol.* **214,** 242–253 (2011).
34. Pecinová, A., Drahota, Z., Nůsková, H., Pecina, P. & Houštěk, J. Evaluation of basic mitochondrial functions using rat tissue homogenates. *Mitochondrion* **11,** 722–728 (2011).
35. Picard, M. *et al.* Mitochondrial structure and function are disrupted by standard isolation methods. *PLoS ONE* **6,** e18317 (2011).
36. Houštěk, J., Cannon, B. & Lindberg, O. Gylcerol-3-phosphate shuttle and its function in intermediary metabolism of hamster brown-adipose tissue. *Eur. J. Biochem.* **54,** 11–18 (1975).
37. Wang, H. *et al.* Resveratrol rescues kidney mitochondrial function following hemorrhagic shock. *Shock* **44,** 173–180 (2015).
38. Porter, C. *et al.* Human and mouse brown adipose tissue mitochondria have comparable UCP1 function. *Cell Metab.* **24,** 246–255 (2016).
39. Feng, D. *et al.* A circadian rhythm orchestrated by histone deacetylase 3 controls hepatic lipid metabolism. *Science* **331,** 1315–1319 (2011).
40. Harms, M. J. *et al.* Prdm16 is required for the maintenance of brown adipocyte identity and function in adult mice. *Cell Metab.* **19,** 593–604 (2014).
41. Kim, D. *et al.* TopHat2: accurate alignment of transcriptomes in the presence of insertions, deletions and gene fusions. *Genome Biol.* **14,** R36 (2013).
42. Liao, Y., Smyth, G. K. & Shi, W. featureCounts: an efficient general purpose program for assigning sequence reads to genomic features. *Bioinformatics* **30,** 923–930 (2014).
43. Robinson, M. D., McCarthy, D. J. & Smyth, G. K. edgeR: a Bioconductor package for differential expression analysis of digital gene expression data. *Bioinformatics* **26,** 139–140 (2010).
44. Chen, E. Y. *et al.* Enrichr: interactive and collaborative HTML5 gene list enrichment analysis tool. *BMC Bioinformatics* **14,** 128 (2013).
45. Kuleshov, M. V. *et al.* Enrichr: a comprehensive gene set enrichment analysis web server 2016 update. *Nucleic Acids Res.* **44** (W1), W90–W97 (2016).
46. Eyre, T. A. *et al.* The HUGO Gene Nomenclature Database, 2006 updates. *Nucleic Acids Res.* **34,** D319–D321 (2006).
47. Kent, W. J., Zweig, A. S., Barber, G., Hinrichs, A. S. & Karolchik, D. BigWig and BigBed: enabling browsing of large distributed datasets. *Bioinformatics* **26,** 2204–2207 (2010).
48. Quinlan, A. R. & Hall, I. M. BEDTools: a flexible suite of utilities for comparing genomic features. *Bioinformatics* **26,** 841–842 (2010).
49. Sequence Read Archive Submissions Staff. Using the SRA Toolkit to convert .sra files into other formats. *SRA Knowledge Base* https://www.ncbi.nlm.nih.gov/books/NBK158900/ (2011).
50. Thorvaldsdóttir, H., Robinson, J. T. & Mesirov, J. P. Integrative Genomics Viewer (IGV): high-performance genomics data visualization and exploration. *Brief. Bioinform.* **14,** 178–192 (2013).
51. Robinson, J. T. *et al.* Integrative genomics viewer. *Nat. Biotechnol.* **29,** 24–26 (2011).
52. Langmead, B., Trapnell, C., Pop, M. & Salzberg, S. L. Ultrafast and memory-efficient alignment of short DNA sequences to the human genome. *Genome Biol.* **10,** R25 (2009).
53. Heinz, S. *et al.* Simple combinations of lineage-determining transcription factors prime cis-regulatory elements required for macrophage and B cell identities. *Mol. Cell* **38,** 576–589 (2010).
54. ENCODE Project Consortium. An integrated encyclopedia of DNA elements in the human genome. *Nature* **489,** 57–74 (2012).
55. Harms, M. J. *et al.* PRDM16 binds MED1 and controls chromatin architecture to determine a brown fat transcriptional program. *Genes Dev.* **29,** 298–307 (2015).
56. Martin, M. Cutadapt removes adapter sequences from high-throughput sequencing reads. *EMBnet.journal* **17,** 10 (2011).
57. Ritchie, M. E. *et al.* limma powers differential expression analyses for RNA-sequencing and microarray studies. *Nucleic Acids Res.* **43,** e47 (2015).
58. Robinson, M. D. & Smyth, G. K. Small-sample estimation of negative binomial dispersion, with applications to SAGE data. *Biostatistics* **9,** 321–332 (2008).
59. Step, S. E. *et al.* Anti-diabetic rosiglitazone remodels the adipocyte transcriptome by redistributing transcription to PPARγ-driven enhancers. *Genes Dev.* **28,** 1018–1028 (2014).

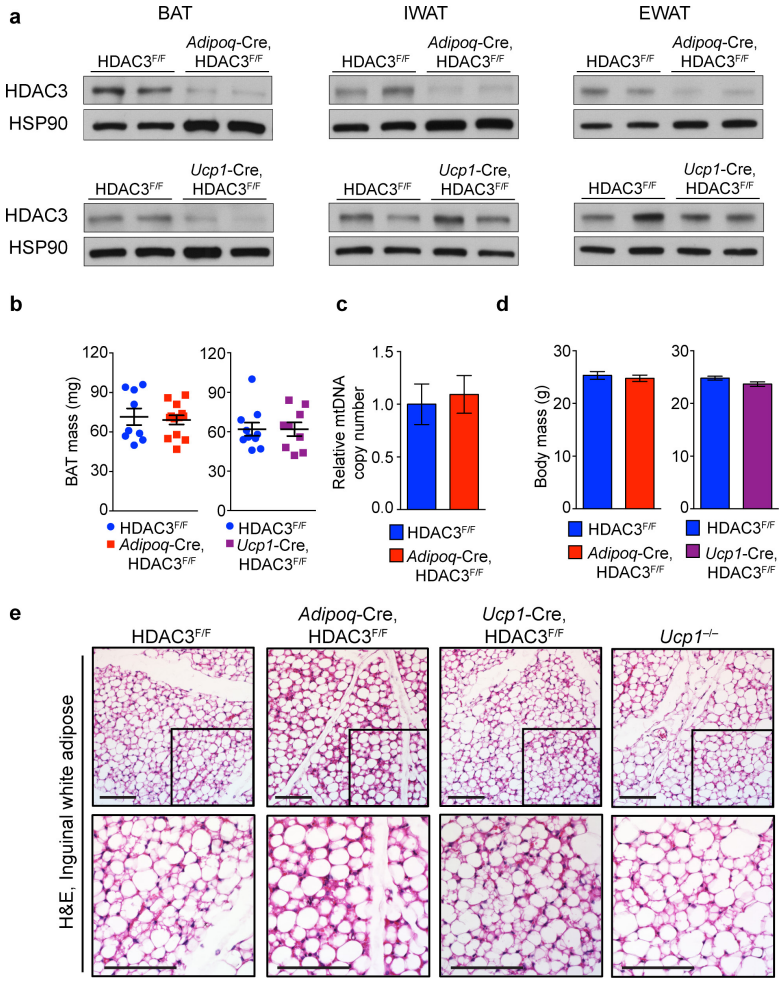

Extended Data Figure 1 | Ablation of HDAC3 in adipose tissue depots. **a**, Immunoblot analysis of interscapular BAT, iWAT, and eWAT of *Adipoq-cre* HDAC3 KO and control littermates, or *Ucp1-cre* HDAC3 KO and control littermates maintained at 22 °C ($n = 2$, all groups) demonstrating tissue-specific conditional KO of HDAC3. **b**–**d**, Interscapular BAT mass (**b**), relative BAT mitochondrial number (**c**), and total body mass (**d**) from *Adipoq-cre* HDAC3 KO and *Ucp1-cre* HDAC3 KO versus control littermates maintained at 22 °C ($n = 13$ *Adipoq-cre*, $n = 9$ control; $n = 9$ *Ucp1-cre*, $n = 10$ control). **e**, Representative haematoxylin and eosin (H&E) staining of inguinal white adipose from 10- to 12-week-old *Adipoq-cre* HDAC3 KO, *Ucp1-cre* HDAC3 KO, *Ucp1* KO, or control mice housed at 22 °C. Lower panels show higher magnification of the boxed areas in upper panels. Scale bars, 100 μm. Data are represented as mean ± s.e.m.

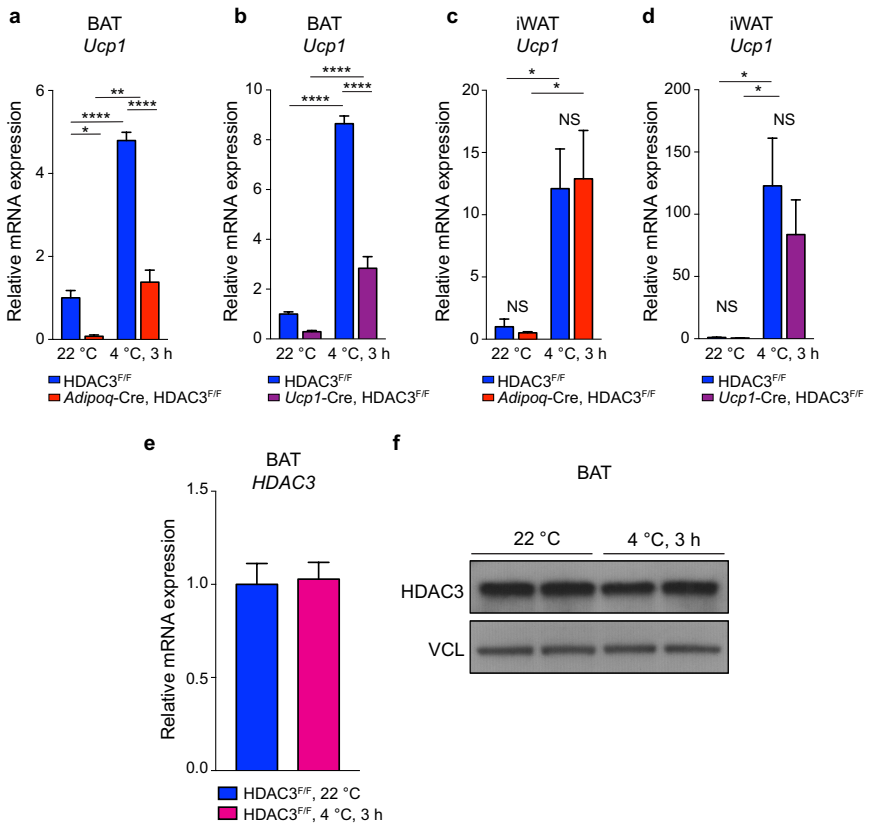

Extended Data Figure 2 | BAT HDAC3 is required for cold-mediated induction of *Ucp1* expression, and HDAC3 expression is not altered by acute cold. a, **b**, BAT *Ucp1* mRNA levels following a 3 h exposure to 4 °C (from 22 °C) versus control littermates maintained at 22 °C in (**a**) *Adipoq-cre* HDAC3 KO versus control ($n = 5, 5$, per temperature) and (**b**) *Ucp1-cre* HDAC3 KO versus control ($n = 5, 5$, per temperature). **c**, **d**, iWAT *Ucp1* mRNA levels following 3 h exposure to 4 °C, versus control littermates maintained at 22 °C in (**c**) *Adipoq-cre* HDAC3 KO versus control ($n = 5, 5$, per temperature) and (**d**) *Ucp1-cre* HDAC3 KO versus control ($n = 5, 5$, per temperature). **e**, BAT *HDAC3* mRNA expression levels following a 3 h exposure to 4 °C (from 22 °C) versus control littermates maintained at 22 °C ($n = 5, 5$, per temperature). **f**, BAT HDAC3 protein levels following 3 h acute cold exposure at 4 °C (from 22 °C) versus control littermates maintained at 22 °C. VCL, vinculin. NS, not significant, $^{*}P < 0.05$, $^{**}P < 0.01$, $^{***}P < 0.001$, $^{****}P < 0.0001$ as determined by a two-way ANOVA with Holm–Šidák's post hoc test (**a**–**d**) or two-tailed Student's *t*-test (**e**). Data are represented as mean ± s.e.m.

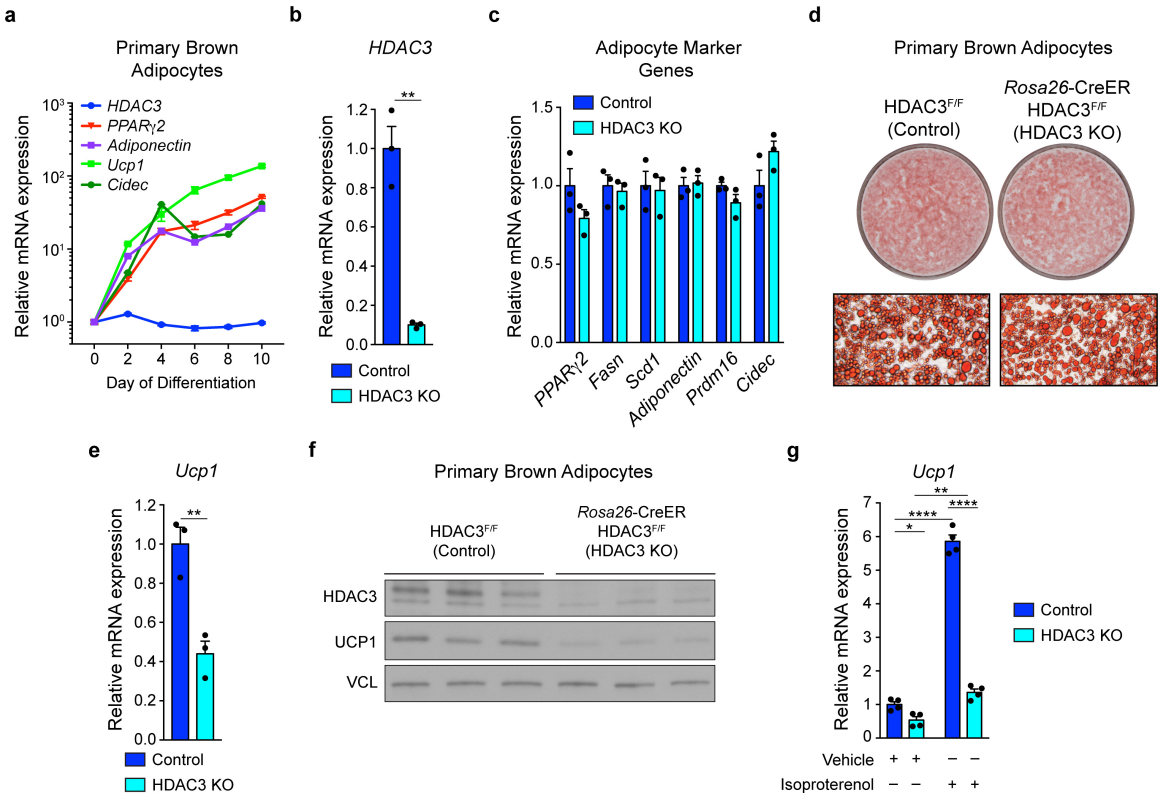

Extended Data Figure 3 | HDAC3 is neither induced nor required for brown adipogenesis, but required for cell-autonomous *Ucp1* expression. a, Gene expression spanning differentiation of cultured WT primary brown adipocytes ($n = 5$ replicates per time point). **b**, Depletion of HDAC3 in day 8 cultured mature brown adipocytes after addition of 2 μm 4-hydroxytamoxifen (4-OHT) during days 0–2 of differentiation to *Rosa26-CreER*-positive (HDAC3 KO) and *Rosa26-CreER*-negative (control) cells derived from littermates ($n = 3, 3$). **c**, Adipocyte-specific gene expression in cultured primary brown adipocytes after depletion of HDAC3 versus control ($n = 3, 3$). **d**, Assessment of lipid accumulation (evaluated by Oil Red-O staining) in cultured HDAC3 KO versus control primary brown adipocytes. **e**, *Ucp1* mRNA expression in cultured primary brown adipocytes after depletion of HDAC3 versus control ($n = 3, 3$). **f**, UCP1 protein expression in cultured primary brown adipocytes after depletion of HDAC3 versus control. ($n = 3, 3$). VCL, vinculin. **g**, *Ucp1* mRNA expression in cultured primary brown adipocytes after depletion of HDAC3 versus control and treated with vehicle (ethanol) or isoproterenol (1 μm) for 3 h ($n = 4$ per group). $^{*}P < 0.05$, $^{**}P < 0.01$, $^{***}P < 0.001$, $^{****}P < 0.0001$, as determined by a two-tailed Student's *t*-test (**b**, **c**, **e**) or by a two-way ANOVA with Holm–Šidák's post hoc test (**g**). Data are represented as mean ± s.e.m.

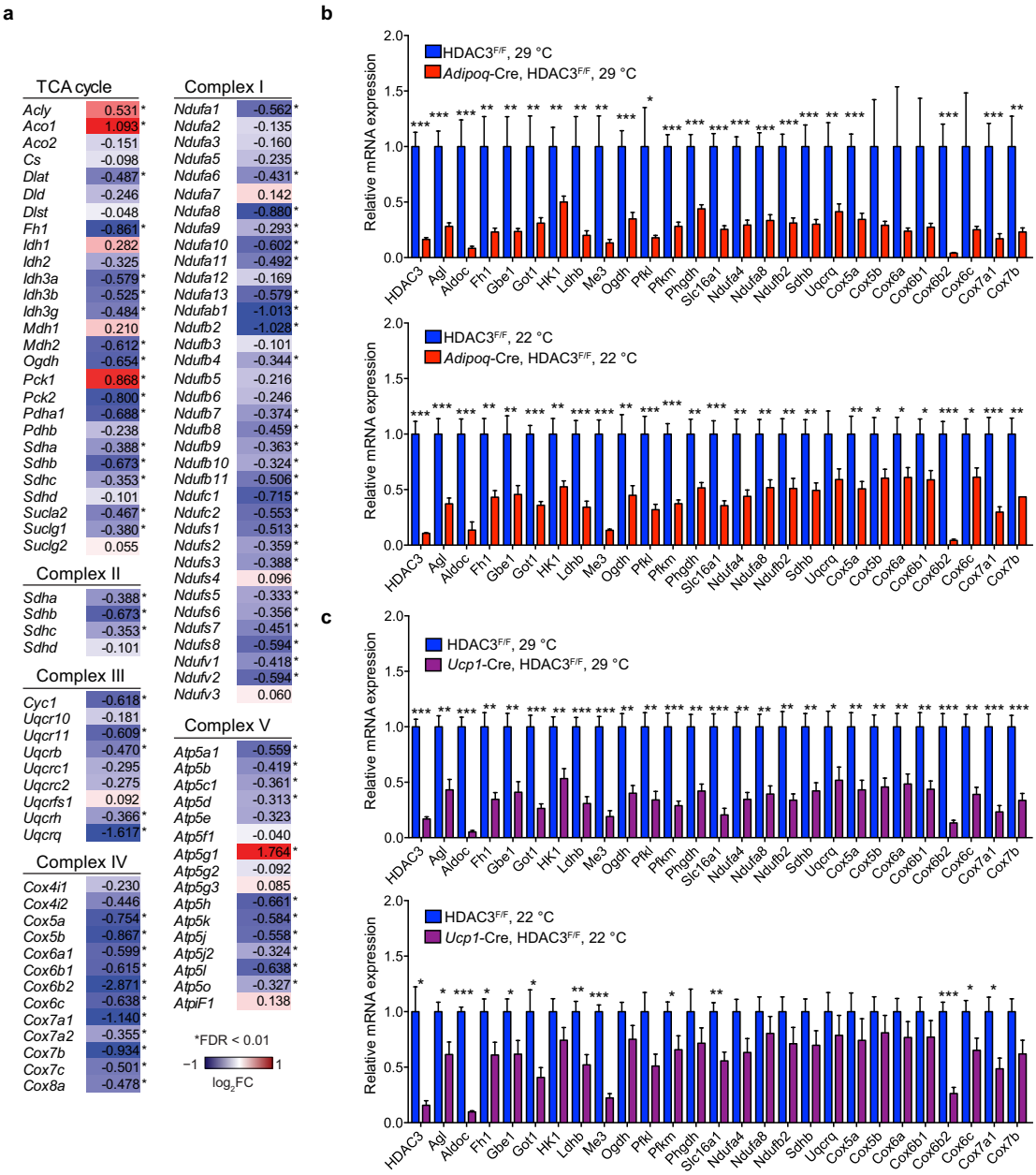

Extended Data Figure 4 | HDAC3 is required for expression of mitochondrial OXPHOS and TCA cycle genes. a, Bioinformatic extension of identified Gene Ontology categories (Fig. 2c) to all oxidative phosphorylation and TCA cycle genes as retrieved by the HUGO gene nomenclature database. *Gene expression change in RNA-seq dataset with an FDR < 0.01. **b**, **c**, RT–qPCR verification of gene expression changes highlighted in Fig. 2d: **b**, *Adipoq-cre* HDAC3 KO versus control littermates at 29 °C (upper, $n = 9, 6$) and 22 °C (lower, $n = 9, 7$); **c**, *Ucp1-cre* HDAC3 KO versus control littermates at 29 °C (upper, $n = 5, 6$) and 22 °C (lower, $n = 5, 7$). *$P < 0.05$, **$P < 0.01$, ***$P < 0.001$, as determined by a two-tailed Student's *t*-test. Data are represented as mean ± s.e.m.

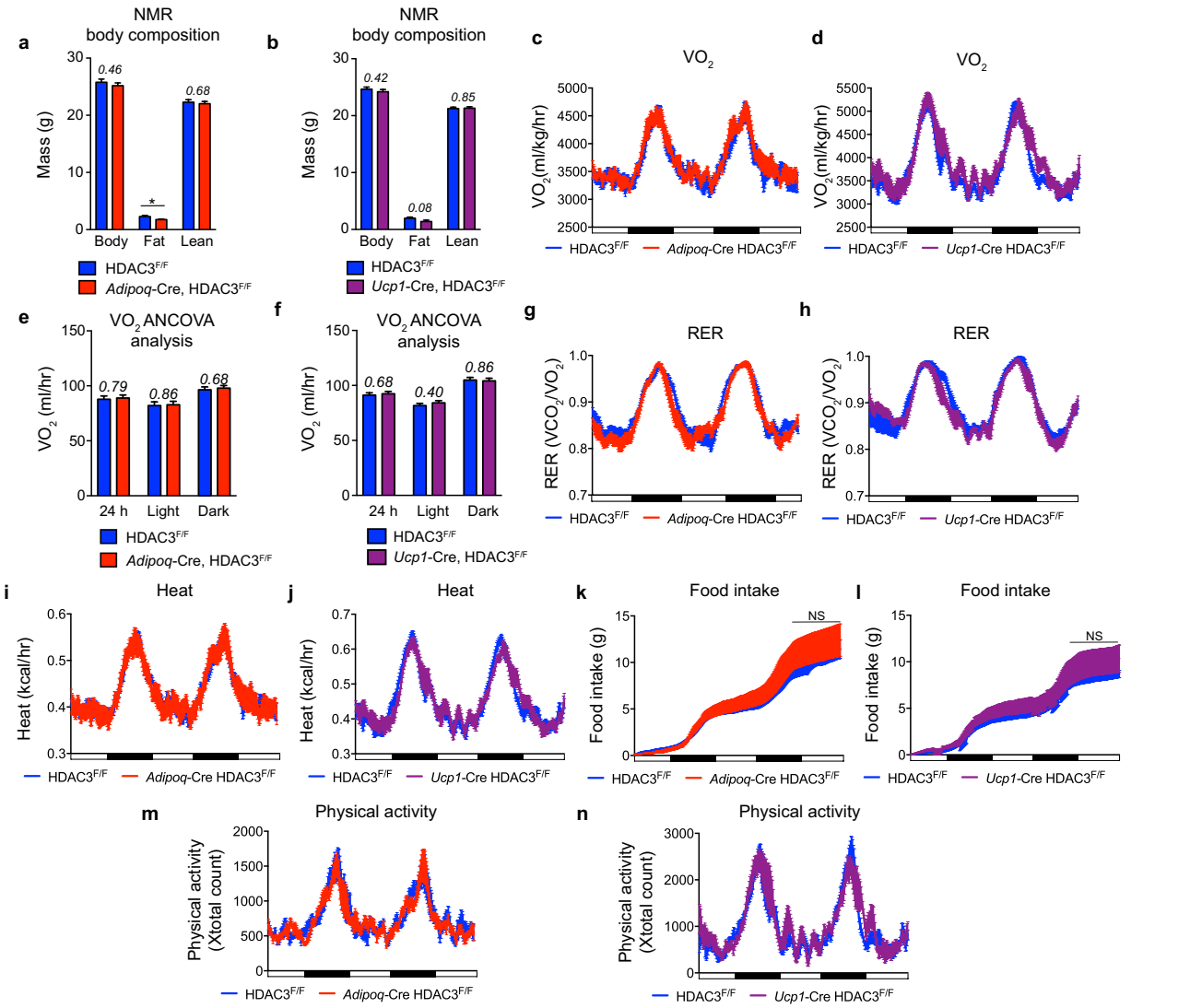

Extended Data Figure 5 | Metabolic studies of *Adipoq-cre* and *Ucp1-cre* HDAC3 KO mouse models. a, **b**, NMR analysis of body composition: **a**, *Adipoq-cre* HDAC3 KO mice versus control littermates ($n = 8, 11$); **b**, *Ucp1-cre* HDAC3 KO mice versus control littermates ($n = 7, 9$). **c**–**n**, CLAMS metabolic cage analysis. **c**, **d**, Oxygen consumption (VO_2): **c**, *Adipoq-cre* HDAC3 KO versus control littermates ($n = 6, 5$); **d**, *Ucp1-cre* HDAC3 KO versus control littermates ($n = 6, 6$). **e**, **f**, ANCOVA of VO_2 (linear regression analysis of total body mass and oxygen consumption): **e**, *Adipoq-cre* HDAC3 KO versus control littermates ($n = 6, 5$); **f**, *Ucp1-cre* HDAC3 KO versus control littermates ($n = 6, 6$). **g**, **h**, Respiratory exchange ratio (RER): **g**, *Adipoq-cre* HDAC3 KO versus control littermates ($n = 6, 5$); **h**, *Ucp1-cre* HDAC3 KO versus control littermates ($n = 6, 6$). **i**, **j**, Heat measurements (kcal h^{-1}): **i**, *Adipoq-cre* HDAC3 KO versus control littermates ($n = 6, 5$); **j**, *Ucp1-cre* HDAC3 KO versus control littermates ($n = 6, 6$). **k**, **l**, Food intake: **k**, *Adipoq-cre* HDAC3 KO versus control littermates ($n = 6, 5$); **l**, *Ucp1-cre* HDAC3 KO versus control littermates ($n = 6, 6$). **m**, **n**, Physical activity: **m**, *Adipoq-cre* HDAC3 KO versus control littermates ($n = 6, 5$); **n**, *Ucp1-cre* HDAC3 KO versus control littermates ($n = 6, 6$). *P* values shown in italics. CLAMS data are graphed as rolling averages. NS, not significant, $^*P < 0.05$ as determined by a two-tailed Student's *t*-test (**a**–**d**, **g**–**n**) or ANCOVA (**e**, **f**). Data are represented as mean ± s.e.m.

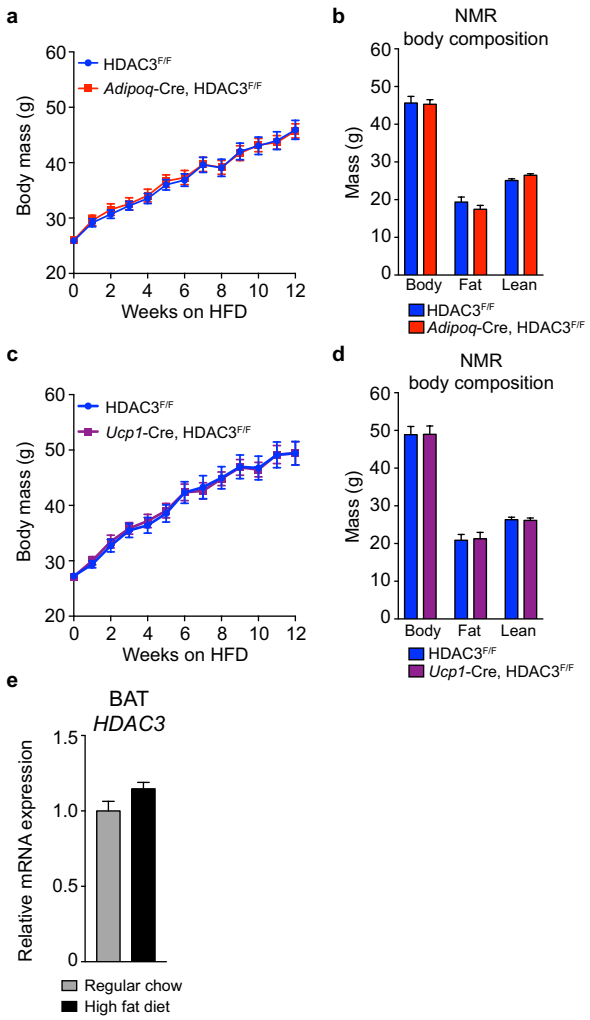

Extended Data Figure 6 | Effect of high-fat diet on *Adipoq-cre* and *Ucp1-cre* HDAC3 KO mouse models. Twelve-week-old weight-matched HDAC3 KO and control littermates were fed high-fat diet (HFD) for 12 weeks. **a**, Weekly body weights, ($n = 8$ *Adipoq-cre*, $n = 10$ control). **b**, Body composition analysis by NMR ($n = 8$ *Adipoq-cre*, $n = 10$ control). **c**, Weekly body weights, ($n = 7$ *Ucp1-cre*, $n = 7$ control). **d**, Body composition analysis by NMR ($n = 7$ *Ucp1-cre*, $n = 7$ control). **e**, RT–qPCR of BAT *HDAC3* mRNA expression after 12 weeks high-fat diet versus controls fed with regular chow ($n = 7, 5$, respectively). Data are represented as mean ± s.e.m.

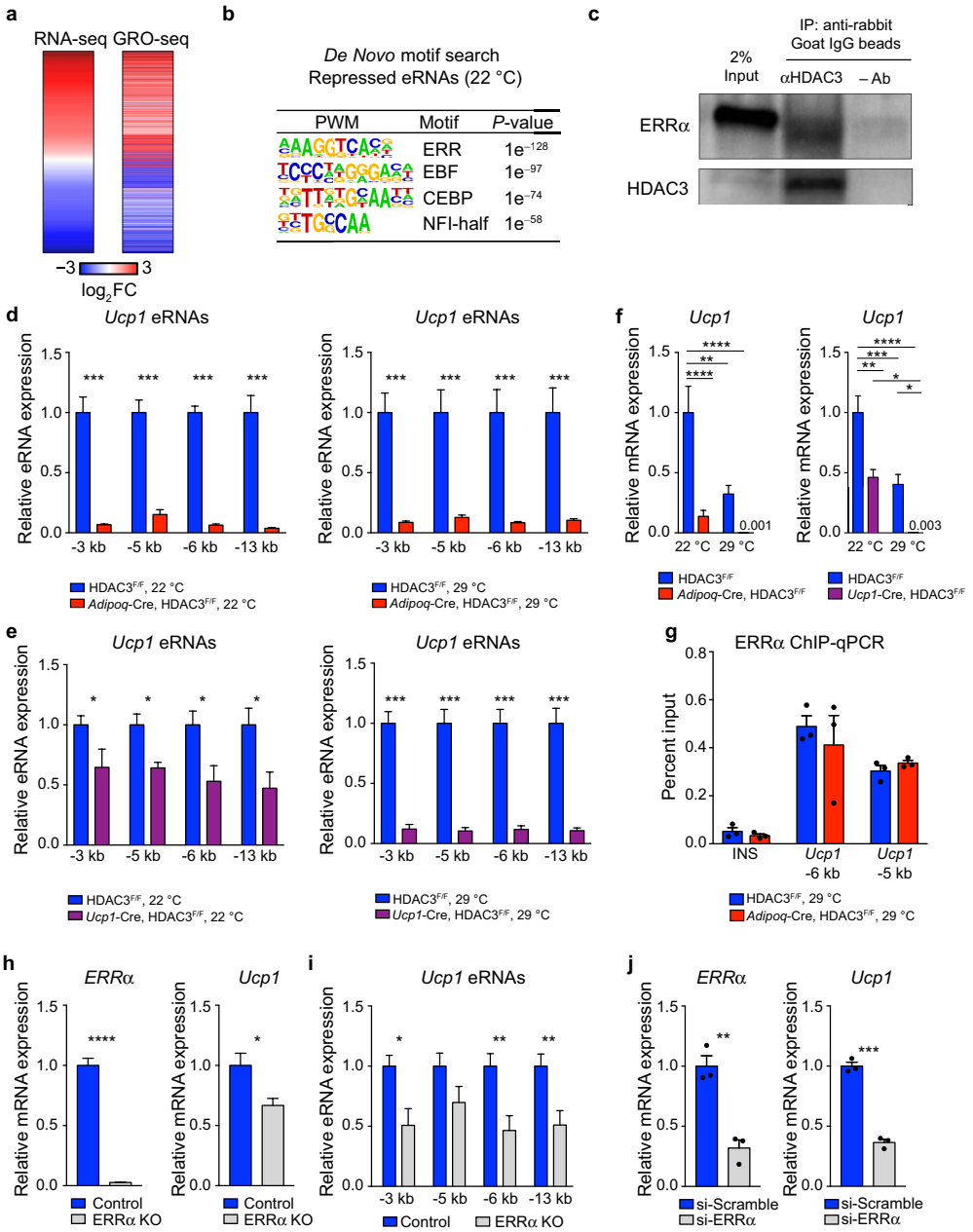

Extended Data Figure 7 | Transcriptional role of HDAC3 and ERRα in BAT. a, Heat map demonstrating correlation of RNA-seq and GRO-seq data. Differentially expressed genes in RNA-seq or GRO-seq data were sorted by $\log_2$(fold change) in RNA-seq. FC, fold change. **b**, *De novo* motif enrichment at repressed eRNAs in *Adipoq-cre*, HDAC3 KO mice versus control littermates ($n = 10, 10$; pooled biological replicates per library) maintained at 22 °C and ranked by *P* value. **c**, Endogenous HDAC3 co-immunoprecipitation of ERRα in differentiated mature brown adipocytes. **d**, **e**, RT–qPCRs of BAT *Ucp1* eRNA expression and (**f**) *Ucp1* mRNA at 22 °C and 29 °C in *Adipoq-cre* and *Ucp1-cre* HDAC3 KO mice versus control littermates, 29 °C ($n = 9$ *Adipoq-cre*, $n = 6$ control; $n = 5$ *Ucp1-cre*, $n = 6$ control) and 22 °C ($n = 9$ *Adipoq-cre*, $n = 7$ control; $n = 5$ *Ucp1-cre*, $n = 7$ control). **g**, ChIP–qPCR of ERRα at *Ucp1* enhancers in *Adipoq-cre* HDAC3 KO versus control littermates ($n = 3, 3$) adapted to 29 °C. **h**, RT–qPCR of *ERRα* and *Ucp1* mRNA expression and (**i**) *Ucp1* eRNA expression in ERRα KO BAT versus control littermates ($n = 8, 7$). **j**, RT–qPCR analysis of *ERRα* and *Ucp1* mRNA expression in mature brown adipocytes after siRNA-mediated knockdown of *ERRα* versus scramble 72 h after transfection ($n = 3, 3$). $^*P < 0.05$, $^{**}P < 0.01$, $^{***}P < 0.001$ as determined by a two-tailed Student's *t*-test (**d**–**e**, **g**–**j**), a two-way ANOVA with Holm–Šidák's post hoc test (**f**). *P* values for motif enrichment as determined by binomial test (**b**). Data are represented as mean ± s.e.m.

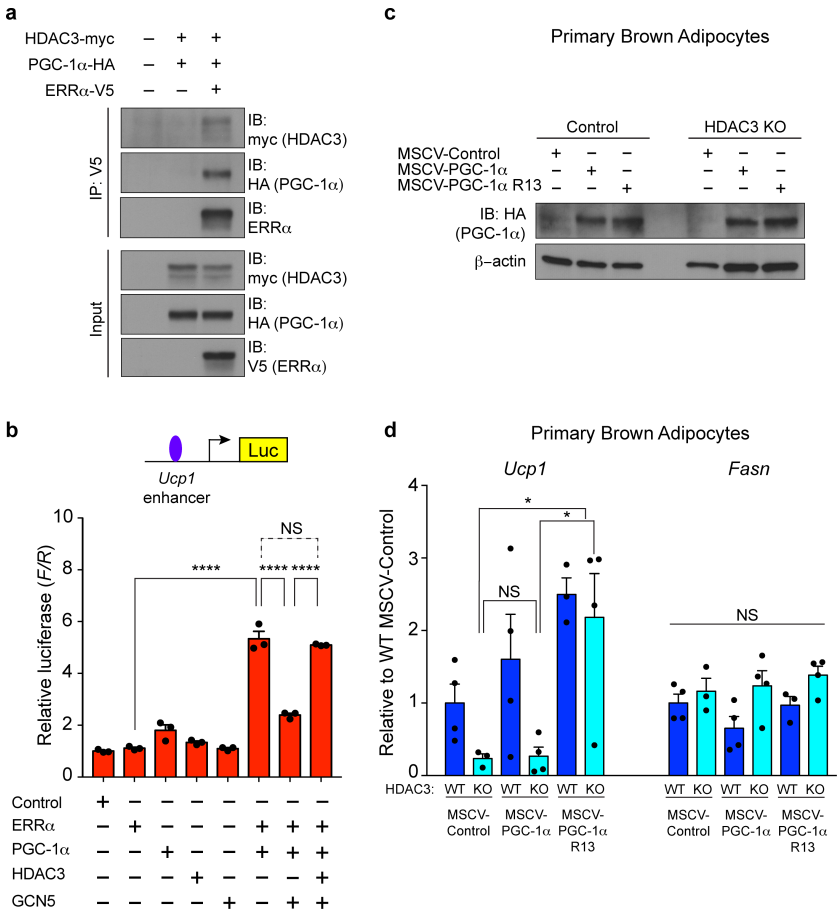

Extended Data Figure 8 | Role of HDAC3 on PGC-1α acetylation and function. a, Co-immunoprecipitation of HDAC3 and PGC-1α with ERRα from HEK-293FT cells. **b**, Luciferase reporter assay of transcription driven by the major *Ucp1* enhancer (−6 kb) after transfection of ERRα, PGC-1α, GCN5, and/or HDAC3 ($n = 3$ replicates per condition). **c**, **d**, Primary brown pre-adipocytes from *Rosa26-CreER*-positive *Hdac3*$^{f/f}$ and *Hdac3*$^{f/f}$ control littermates transduced with MSCV retroviruses: control, PGC-1α WT, or non-acetylatable PGC-1α R13 mutant, treated with 2 μm 4-hydroxytamoxifen during days 0–2 of differentiation to deplete HDAC3, and studied at day 8 of differentiation. **c**, Immunoblot analysis of exogenous PGC-1α expression in primary brown adipocytes ($n = 2$ replicates pooled per lane). **d**, RT–qPCR analysis of *Ucp1* and *Fasn* expression in control and HDAC3 KO primary brown adipocytes following transduction with MSCV-Control ($n = 4$ control, 3 HDAC3 KO), MSCV-PGC-1α WT ($n = 4$ control, 4 HDAC3 KO), or MSCV-PGC-1α R13 (non-acetylatable mutant) ($n = 3$ Control, 4 HDAC3 KO). $^*P < 0.05$, $^{**}P < 0.01$, $^{***}P < 0.001$, $^{****}P < 0.0001$, as determined by a one-way ANOVA with a Tukey's post hoc test (**b**, **d**). Data are represented as mean ± s.e.m.

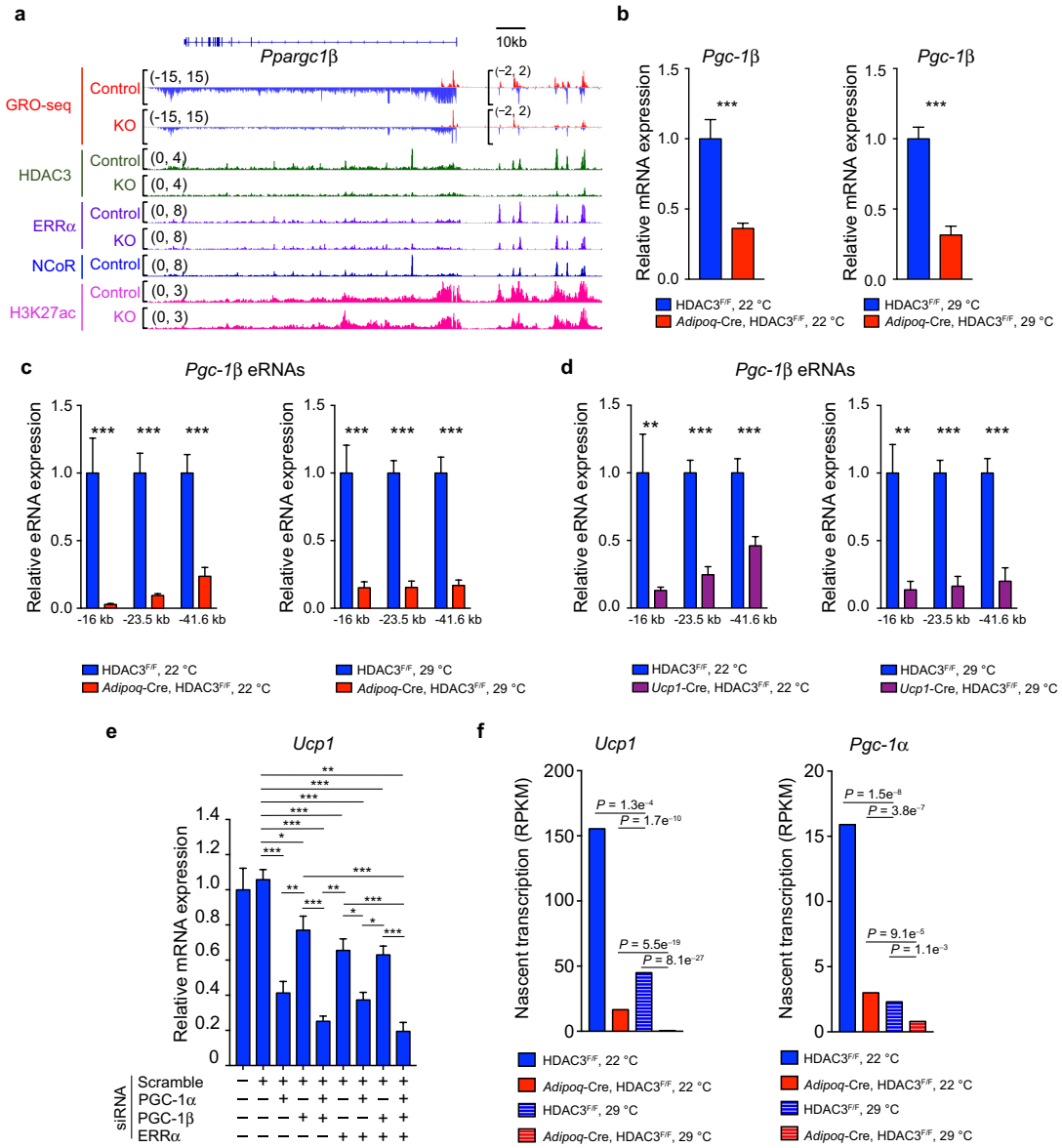

Extended Data Figure 9 | HDAC3 and ERRα activate *Ppargc1b* enhancers and transcription. a, Genome browser tracks of the *Ppargc1b* locus highlighting GRO-seq and ChIP–seq data from HDAC3 KO and control BAT (*y* axis scales, normalized reads, reads per million) demonstrating co-binding of HDAC3, ERRα, and NCoR at functional enhancers. **b**, BAT *Ppargc1b* mRNA levels in *Adipoq-cre* HDAC3 KO BAT versus control littermates (29 °C: $n = 9, 6$; 22 °C: $n = 9, 7$). **c**, **d**, RT–qPCR of eRNAs found at HDAC3 and ERRα enhancers in *Adipoq-cre* HDAC3 KO BAT versus control littermates (29 °C: $n = 9, 6$; 22 °C: $n = 9, 7$) and *Ucp1-cre* HDAC3 KO BAT versus control littermates (29 °C: $n = 5, 6$; 22 °C: $n = 5, 7$). **e**, RT–qPCR analysis of *Ucp1* mRNA expression in mature brown adipocytes after combinatorial siRNA knockdown of *Pgc-1α*, *Pgc-1β*, and/or *ERRα* versus scramble siRNA ($n = 5$ replicates per condition). Statistical analysis performed among groups transfected with siRNAs. **f**, Quantification of *Ucp1* and *Pgc-1α* nascent gene body transcription (GRO-seq) at 22 °C and 29 °C in *Adipoq-cre* HDAC3 KO BAT versus control littermates ($n = 10, 10$, pooled biological replicates per library). $^*P < 0.05$, $^{**}P < 0.01$, $^{***}P < 0.001$, as determined by a two-tailed Student's *t*-test (**b**–**d**), one-way ANOVA with a Holm–Šidák post hoc test (**e**), or an exact test (performed in EdgeR). Data are represented as mean ± s.e.m.